Development of Technique to Measure Instantaneous Slip Between Cam and Roller in Real Engine

Author

SOBAN AHMAD SAIR

Registration Number

205850

Supervisor

Prof. Dr RIAZ AHMAD MUFTI

DEPARTMENT

SCHOOL OF MECHANICAL & MANUFACTURING ENGINEERING

NATIONAL UNIVERSITY OF SCIENCES AND TECHNOLOGY

ISLAMABAD

AUGUST 2017

Development of Technique to Measure Instantaneous Slip Between Cam and Roller in Real Engine

Author

SOBAN AHMAD SAIR

Registration Number

205850

A thesis submitted in partial fulfillment of the requirements for the degree of

MS Mechanical Engineering

Thesis Supervisor:

Prof. Dr RIAZ AHMAD MUFTI

Thesis Supervisor's Signature: _____

DEPARTMENT

SCHOOL OF MECHANICAL & MANUFACTURING ENGINEERING

NATIONAL UNIVERSITY OF SCIENCES AND TECHNOLOGY,

ISLAMABAD

AUGUST 2017

Declaration

I certify that this research work titled "*Development of Technique to Measure Instantaneous Slip Between Cam and Roller in Real Engine"* is my own work. The work has not been presented elsewhere for assessment. The material that has been used from other sources it has been properly acknowledged / referred.

Signature of Student

SOBAN AHMAD SAIR

Registration Number

205850

Proposed Certificate for Plagiarism

It is certified that MS Thesis Titled "**Development of Technique to Measure Instantaneous Slip Between Cam and Roller in Real Engine**" by **Soban Ahmad Sair** has been examined by us. We undertake the follows:

a. Thesis has significant new work/knowledge as compared already published or are under consideration to be published elsewhere. No sentence, equation, diagram, table, paragraph or section has been copied verbatim from previous work unless it is placed under quotation marks and duly referenced.
b. The work presented is original and own work of the author (i.e. there is no plagiarism). No ideas, processes, results or words of others have been presented as Author own work.
c. There is no fabrication of data or results which have been compiled/analyzed.
d. There is no falsification by manipulating research materials, equipment or processes, or changing or omitting data or results such that the research is not accurately represented in the research record.
e. The thesis has been checked using TURNITIN (copy of originality report attached) and found within limits as per HEC plagiarism Policy and instructions issued from time to time.

Name & Signature of Supervisor

Prof. Dr Riaz Ahmad Mufti

Signature **:** _____

Plagiarism Certificate (Turnitin Report)

Development of Technique to measure instantaneous slip

ORIGINALITY REPORT

6%	0%	6%	2%
SIMILARITY INDEX	INTERNET SOURCES	PUBLICATIONS	STUDENT PAPERS

PRIMARY SOURCES

1	Shivam Alakhramsing, Matthijn de Rooij, Aydar Akchurin, D.J. Schipper, Mark van Drogen. "A mixed-TEHL analysis of cam-roller contacts considering roller slip: On the influence of rollerpin contact friction", Journal of Tribology, 2018 Publication	1%
2	Muhammad Khurram, Riaz A Mufti, Rehan Zahid, Naqash Afzal, Usman Bhutta. "Experimental measurement of roller slip in endpivoted roller follower valve train", Proceedings of the Institution of Mechanical Engineers, Part J: Journal of Engineering Tribology, 2015 Publication	1%

3	Shivam S Alakhramsing, Matthijn B de Rooij, Mark van Drogen, Dirk J Schipper. "The influence of stick–slip transitions in mixedfriction predictions of heavily loaded cam–roller contacts", Proceedings of the Institution of Mechanical Engineers, Part J: Journal of Engineering Tribology, 2018 Publication	1%
5	Muhammad Khurram, Riaz Ahmad Mufti, Muhammad Usman Bhutta, Naqash Afzal et al. "Roller sliding in engine valve train: Effect of oil film thickness considering lubricant composition", Tribology International, 2019 Publication	1%

Signature of Student

SOBAN AHMAD SAIR

Registration Number

205850

Signature of Supervisor

_____

FORM TH-4

MASTER THESIS WORK

We hereby recommend that the dissertation prepared under our supervision by: (Student Name & Regn No.)_Soban Ahmad Sair & 205850 Titled: **Development of Technique to Measure Instantaneous Slip Between Cam and Roller** in Real Engine be accepted in partial fulfillment of the requirements for the award of **Master's in Mechanical Engineering** degree.

Examination Committee Members

1. Name: Dr Jawad Aslam Signature:_____

2. Name: Dr Mian Ashfaq Ali Signature:_____

3. Name:Dr Rehan Zahid Signature:_____

Supervisor's name: **Prof. Dr Riaz Ahmad Mufti** Signature:_____

Date:_____

_____ _____

Head of Department Date

COUNTERSINGED

_____

Dean/Principal

Date:_____

Copyright Statement

Acknowledgements

I am thankful to my Creator Allah Subhana-Watala to have guided me throughout this work at every step and for every new thought which I setup in my mind to improve it. Indeed, I could have done nothing without Your priceless help and guidance. Whosoever helped me throughout the course of my thesis, whether my parents or any other individual was Your will, so indeed none be worthy of praise but You.

I am profusely thankful to my beloved parents who raised me when I was not capable of walking and continued to support me throughout in every department of my life.

Writing the acknowledgements marks the end of an extensive and fruitful period of research. The work herein is highly attributable to several academia people. I eagerly would like to take this opportunity to thank these people. First, I would like to thank my supervisor Prof. Dr Riaz Ahmad Mufti for his valuable input and motivation during this project and giving me the freedom and chance to do the present research independently.

Secondly, I would like to thank my co-supervisor Dr. Jawad Aslam for his valuable inputs and mostly harsh comments from time to time. His input always reminded me of the context in which the present work was placed, and hence closely kept me to the scope of the project.

Thirdly, I am also thankful to my colleagues Waleed Bin Khalid, Uzair Ahmad, Shahzeb Aamir to help me develop new technique. Especial thanks to Fazal Badshah, Talha Yousaf and Rehan bin Safeer, for their valuable technical support and suggestions. A big thanks to Mr. Nisar, Mr. Aqseer and Mr. Waseem at the MRC department with regards to the manufacturing and instrumentation phase.

Finally, I would also like to extend my appreciation to the committee members Dr Sami-Ur-Rehman Shah, Dr Mian Ashfaq, Dr Rehan Zahid for their time and effort.

Dedicated to my exceptional parents and adored siblings whose tremendous support and cooperation led me to this wonderful accomplishment.

ABSTRACT

End-pivoted roller followers are a common type of valve actuation configurations in modern passenger vehicles. Considerable research work has gone into such valve actuation configurations with regards to average roller slippage, roller friction, and oil pressure, however, limited work has been done on the measurement of instantaneous slip.

In this study, an instrumentation method is developed and implemented to study how irregular roller movements relative to the cam vary instantaneously. The technique avoids any major modifications to the rollers and test engine, allowing us to detect slip while simulating a live engine. Using this experimental technique, one can investigate instantaneous roller slip by studying the effects of different variables such as lubricant type, surface finish, temperature, cam profile and rotation speed.

Key Words: *End-pivoted roller follower, AlNiCo Magnets, Instantaneous Slip, Giant Magneto resistive Sensor*

ABBREVIATIONS

GMR	Giant Magneto-resistance
TMR	Tunnel Magneto-resistance
AlNiCo	Aluminum Nickle Cobalt
CNC	Computerized Numeric Control
DAQ	Data Acquisition
mm	Millimeter
RPM	Revolutions per Minute
Hz	Hertz
AWG	American Wire Gauge

NOMENCLATURE

Oe	Oersted unit of the auxiliary magnetic field in the centimeter–gram
V_{DD}	Supply Voltage
GND	Ground Connection
NC	No Connection
$\emptyset$	Diameter

CHAPTER 1: INTRODUCTION

1.2 Problem statement

Consumer demands, environmental protection and government mandate are all factors which are accelerating the development of more fuel-efficient vehicles. Heavy-duty vehicles such as trucks, buses and coaches produce around 25% of CO2 emissions from road transport in the EU and around 6% of the EU's total CO2 emissions [1]. In order to contribute to the achievement of the EU's commitments under the Paris Agreement [2] the EU has set out mandatory targets, one of which is that the average CO2 emissions of new heavy-duty vehicles will have to be 15% lower in 2025 than in 2019 [1].

In order to achieve these strict fuel efficiency requirements without degradation of vehicle performance, vehicle manufacturers have been making significant hardware modifications such as better vehicle aerodynamics, engine downsizing, usage of lightweight materials and low rolling resistance tires. Another way of improving the fuel economy is by reducing the internal friction losses of the engine. Air inlet and exhaust in automobile engines is controlled via the actuation of the inlet and exhaust valves of the engine cylinder. These inlet and exhaust valve movements are controlled by the rotation of cam shafts which is in contact with followers. These followers can be of many types with different coating materials used on the roller surface which comes in direct contact with the cam surface Thus, lubricant manufacturers have also developed highly advanced lubricants to reduce engine friction losses. Lubricants that are fuel-efficient are often formulated using high-quality low-viscosity base oils with advanced additive technologies. Downsizing engines means increasing the power density, due to their smaller size and higher output, and thus increasing loads on mechanical components. This, together with the use of even lower viscosity oils, causes main engine components to operate under harsh conditions, which may eventually lead to accelerated surface wear and thus ultimately to a shortened engine life. Cam-roller followers as part of valve -train mechanisms in internal combustion engines are of crucial importance. Figure 1.1 and 1.2 shows an example of a camshaft and a roller follower unit.

Figure 1.1: Camshaft

Figure 1.2: roller follower assembly

Anderson [3] reported that the valve train mechanism accounts for 6-10% of the internal engine friction losses. The cam-roller contact is a lubricated contact, experiencing highly dynamic and/or abruptly varying operational conditions in terms of load and velocity, coming from the camshaft that drives it. To elaborate somewhat, this contact is subjected to very high pressures coming from the fuel injector. Peak pressure values of 2 GPa are not uncommon. Related to this, the degree of separation between surfaces, defined as specific film thickness, has a very strong influence on the type and amount of wear.

Figure 1.3: Cam experiencing adhesive wear at **(a)** initial stage and **(b)** a more progressed stadium

Ideally the movement between cam and follower is without slippage and the time intervals are constant between each position. In certain cases, however, the roller movement can experience a lag with respect to the cam movement due to slippage or it may move ahead of the cam due to inertial movements [4]. Slippage or inertial movements results in changes in the combustion process as the valve opening and closing now do not perfectly match the desired actuation timings. In order to measure the instantaneous intensity of these variations (slippage/inertial movements) with respect to different parameters such as follower types and different roller materials, we used various instrumentation techniques to find out the variations.

1.3 The Followers

Different types of followers and followers with rollers of different surface coating were to be instrumented in order to compare the results. The following is the list of rollers that we had:

1) DAF Truck Tappet Roller
2) Toyota Prius Finger Follower

1.3.1 DAF Truck Tappet Follower

The Roller from DAF was a bush type Tappet Follower and had three parts.

1) Roller Casing
2) Roller Axis
3) Roller Bush

Figure 1.4: DAF Tappet Follower

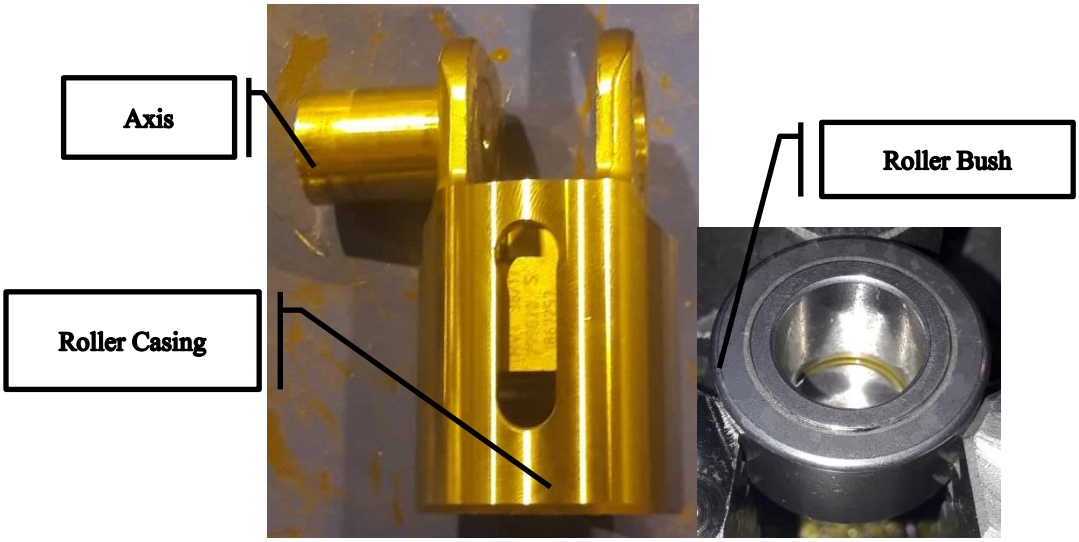

Figure 1.5: Parts of DAF Tappet Follower

The dimensions of the roller are as mentioned below:

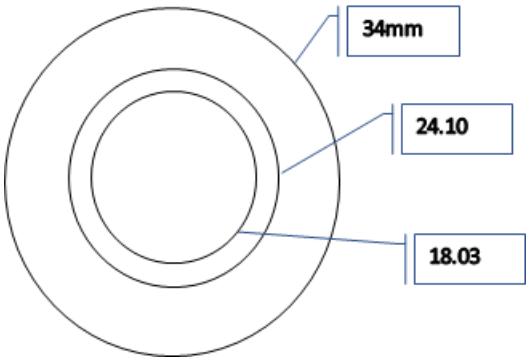

Figure 1.6: Roller Dimensions (all dimensions in mm)

This type of follower uses simple lubrication between the roller (bush) and the axis instead of depending on bearings of any kind.

1.3.2 Prius End Pivoted Finger Follower Roller

This roller had four parts:

1) Roller Casing
2) Roller Axis
3) Roller

4) Needle Bearings

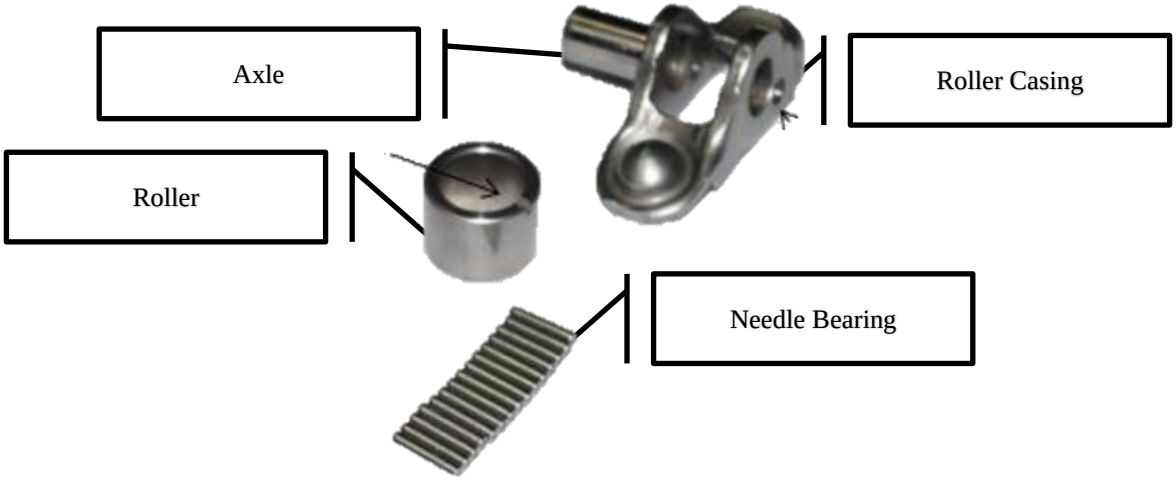

Figure 1.7: Parts of Toyota Prius Follower

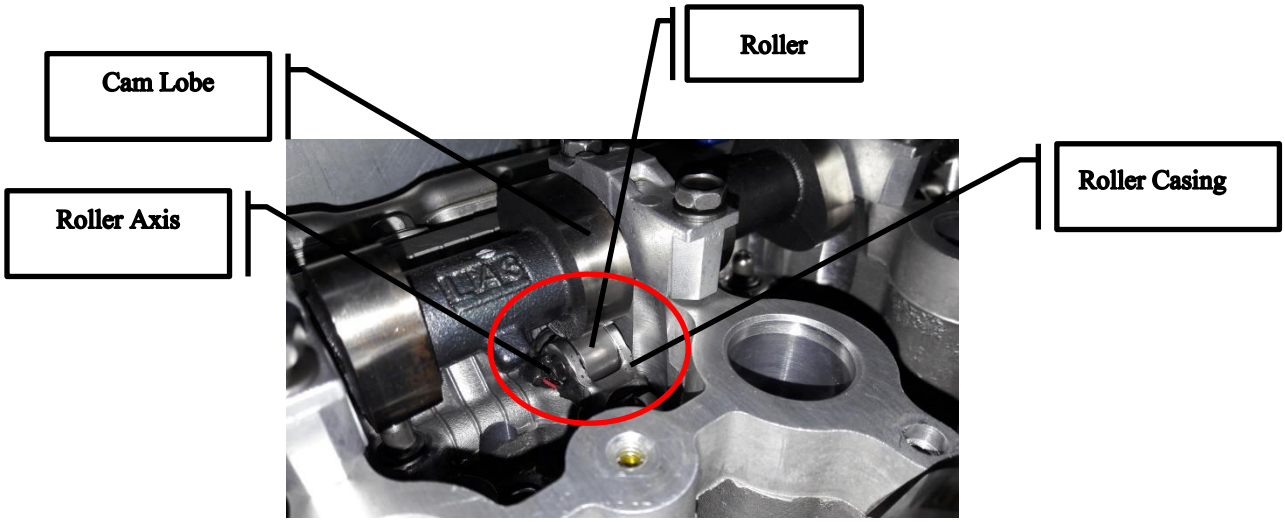

Figure 1.8: Finger Follower Roller

The dimensions of the roller are as given below:

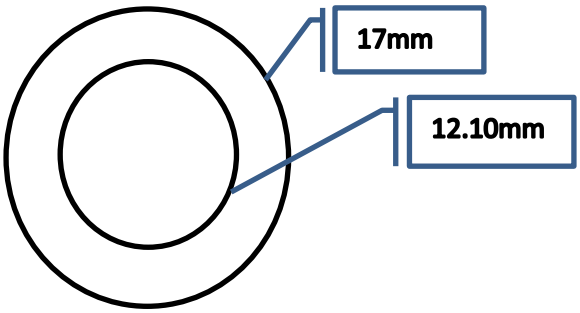

Figure 1.9: Dimensions of Toyota Prius Roller

Comparatively, this roller is much smaller in size as compared to the DAF Truck roller which is why different instrumentation techniques were used for both the rollers which are discussed in subsequent sections.

1.4 The Approach

To find out precise locations at which the roller experienced slippage or inertial movements, it was important to divide the roller into parts via instrumentation and assess when each part crossed a certain checkpoint, which would be our sensor. This would form a tachometer of sorts. Essentially, once the roller would be divided in equal parts, we would know when a certain part crosses the checkpoint. In ideal conditions all divided parts would cross the checkpoint at equal time intervals, however disruption in this pattern would signify irregularities in the cam and follower interaction.

Figure 1.10: Roller Movement Detection Concept

We considered various approaches to instrument the follower assembly such as Hall Effect sensor with magnets embedded in the roller, visual inspection by high speed camera et cetera; however, these methods were shown to be inefficient in previous experiments of a similar nature such as Khurram et al. [5]. We were now down to two options, i.e. using either a GMR sensor or a TMR sensor.

A general outline of the instrumentation the procedure via GMR sensors (sensor method found to be most feasible) is given below:

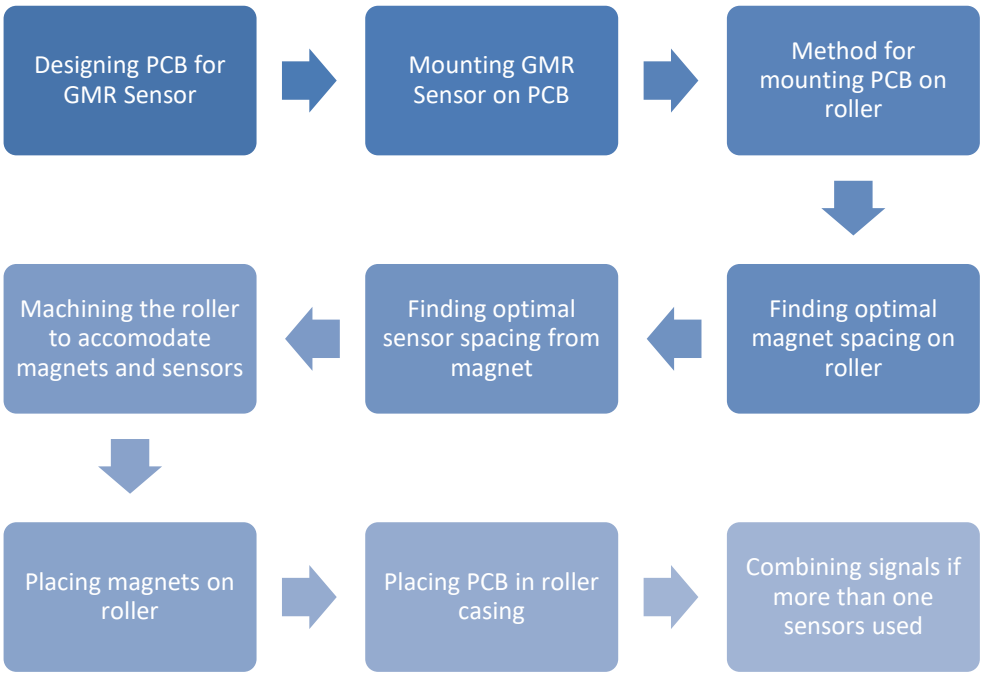

Figure 1.11: Step by Step Instrumentation Process

CHAPTER 2: LITERATURE REVIEW

The cam-roller follower unit as a tribo-system is inherently a coupling between two lubricated contacts, namely the cam-roller contact and the roller-pin contact. From past literature [6,7] one may observe that significant theoretical and experimental work, in terms of lubrication behavior, has been carried out for cam-flat faced follower configurations (which are simple sliding contacts). This in contrast to the cam-roller follower unit which has gained less attention

Now-a-days, the roller-follower configurations are popular due to their increased tribological efficiency due to rolling instead of sliding contact. Roller rotation minimizes the chances of fatigue failure by even distribution of wear, improves the lubrication, and influences the valve train power loss.

Roller slippage, which strongly governs the frictional force/traction at the cam-roller contact, has been proven experimentally by Duffy [8] and more recently by Khurram et al. [5]. Lee and Patterson [9] reported that the problem of wear still exists if slip occurs. The roller rotational velocity is a function of the torques acting on the roller itself (see Figure 1.7).

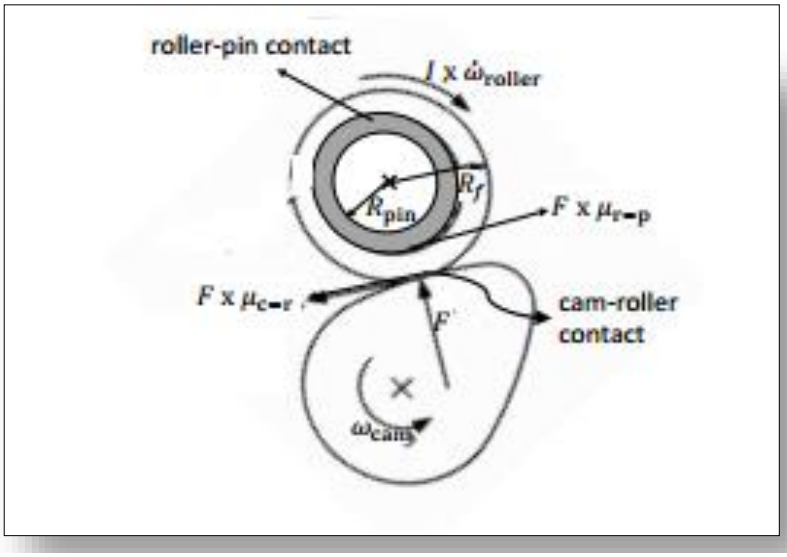

Figure 2.1: Cam-roller follower configuration showing the frictional forces acting at the cam-roller and roller-pin contact.

However, most previous studies (see for instance ([10, 11]) assumed pure rolling conditions at the cam-roller contact, i.e. $U_c = U_r$. Where U_c and U_r are the cam and roller surface velocities at the point of contact.

Chiu [12] and later Ji and Taylor [13] were among the first to develop theoretical lubrication models that consider variable roller rotational velocity at the cam roller contact. A fixed coefficient of friction was assumed for the roller-pin contact. Both the afore mentioned studies determined roller slip at high cam rotational velocities due to simultaneous increase in roller angular momentum. Bair [14] demonstrated in his experiments that roller slippage is strongly governed by the acting contact force, i.e. a higher contact force decreases possible roller slippage due to enhanced traction at the cam-roller contact.

Mixed lubrication conditions were considered by Turturro et al. [15], who presented a steady-state model for a non-Newtonian lubricant to study the effect of viscosity on the friction at cam-roller contact. Khurram et al. [16] studied experimentally the effect of lubricant rheology on average roller slip. In that study they highlighted the effect of viscosity improvers on roller slip.

Umar et al. [17] developed a mixed lubrication model in which they analyzed the effect of flash temperature on cam-follower friction. They compared the sliding and roller follower type configurations and concluded that in both configurations surface roughness plays an important role. Also, the resultant contact temperature was much higher in the case of sliding followers due to higher sliding velocity and friction. In line with this, Abdullah et al. [18] recently investigated the effects of specialized surface treatments on roller slippage. They observed considerable reduction in roller slippage. It is worth mentioning that most of the previously mentioned studies only considered lightly to moderately loaded cam-roller follower contacts, i.e. pressures up to 0.7 GPa approximately. Injection camshafts, which experience much higher pressures (up to 2 GPa), have been studied by Lindholm et al. [19]

Khurram et al. [5] studied tribological effects of end-pivoted roller follower valve train under realistic environment in a Toyota INZK engine and developed a method of instrumenting end pivoted finger follower rollers for experimental data collection. Further studies on the effects of oil

rheology, lubricant chemistry was conducted at different operating conditions using a similar instrumentation approach in [16, 20].

The aforementioned researches made use of the relatively recent giant magneto-resistive (GMR) technology. With the introduction of GMR sensors their application in the automotive industry is increasing as noted by Kasper et al. [21]. Some other instrumentation techniques are also discussed in Treutler et al. [22] where the feasibility of incorporating sensor technologies such as hall effect sensors, reed switches and optical fiber cables is discussed. We went through a detailed study of all methods available to us before narrowing down to our desired mode of instrumentation. Different researches have used different instrumentation methods depending on their requirements and constraints.

1.1 Identified research gap

From the literature review briefly described in the previous section one may conclude that significant effort has been made in order to understand the tribological behavior of cam-roller units better. However, there are still certain topics which are despite their high relevance – not fully covered yet in the literature

Our study aims to bridge that gap for which we devised an instrumentation method that can detect instantaneous slip between the cam roller interaction. In this study, we will look at the design concept for instrumenting the Toyota Prius end-pivoted follower, followed by implementing the approach while making minimal mechanical changes to the roller to embed the sensors.

CHAPTER 3: ENGINE HEAD TEST RIG

The Engine

A real production Toyota 1NZK engine employing end pivoted roller finger follower valve train with overhead camshaft arrangement as shown in figure 5.1 has been instrumented. It is a four cylinders engine with twin cams having 16 valves employing end pivoted roller finger followers for valve actuation with hydraulic lash adjusters. The oil channel available in the engine head cover has small holes as shown in figure 5.2

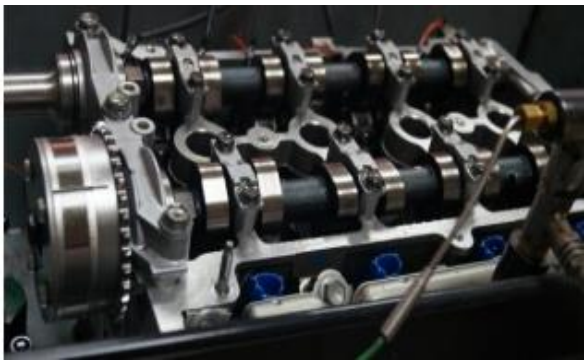

Figure 3.1: Instrumented Toyota 1NZK engine head

Figure 3.2: Engine head cover having oil spray channel

which sprays oil on the camshaft for lubrication purpose. Fig.3.1 Instrumented Toyota 1NZK engine head Fig 3.2 Engine head cover having oil spray channel One end of roller finger follower assembly is pivoted on the hydraulic lash adjuster assembly whereas the other end is seated on the valve cap to operate the valve against the spring tension. The hydraulic lash adjuster maintains zero clearance between the cam lobe and the roller follower during operation. The schematic of under research end pivoted roller finger follower valve train.

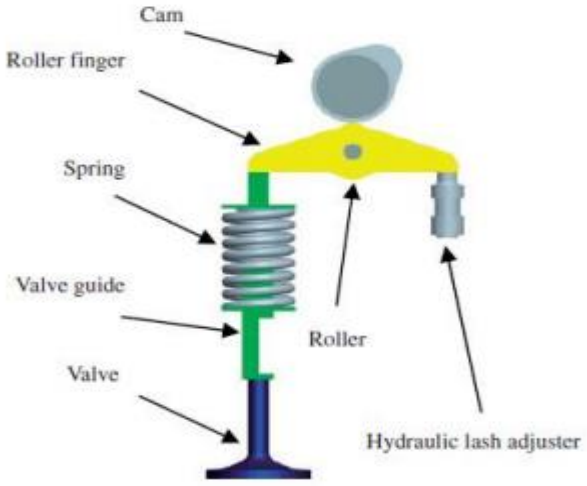

Figure 3.3: Schematic of roller finger follower valve train

The Test Rig

An advanced, flexible and stable engine valve train test rig has been developed in this research work as shown in figure 5.4. In order to limit the vibrations which may be induced during the operation, the engine head was bolted firmly on the test steel plate and then to the rig stand. Anti-vibration mounts are fixed on each leg of test rig stand to reduce noise and absorb vibrations. The engine head was placed in an oil tray, which was in turn connected to the oil sump. The exhaust camshaft was driven through a mechanical coupling by an electrical motor via a feedback controlled variable speed vector flux driver. The bellow coupling is capable of transmitting the backlash free torque and compensate for axial, radial and angular shaft misalignment. The variable speed induction motor is connected to the controller which in turn is connected to the data acquisition system. The speed of the motor can be controlled with the help of a controller PARKER 6054 through computer-based data acquisition system to vary the camshaft speed which ranges up to 3000 rpm. The camshaft speed can be monitored on the computer screen. An optical encoder was also installed at the back of the electrical motor which gave one pulse per half degree of the camshaft revolution resulting 720 degrees in a complete operating cycle.

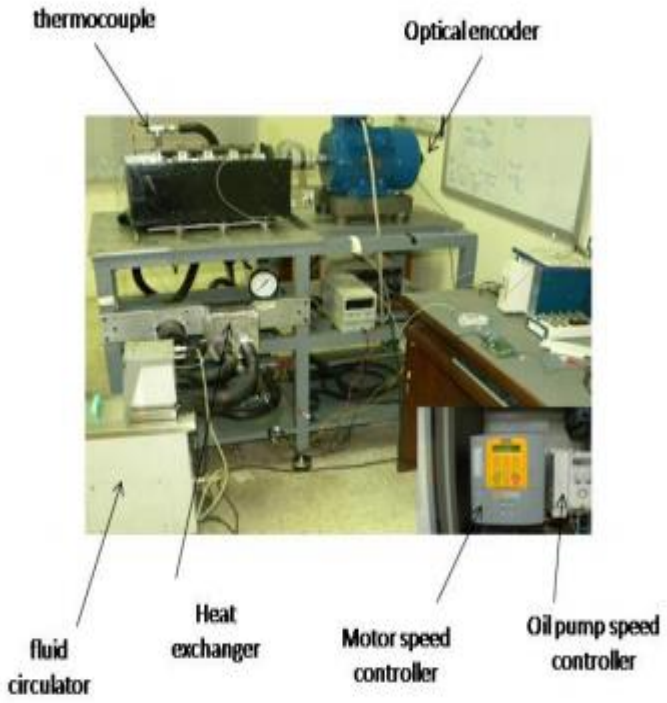

Figure 3.2: Advanced flexible test rig

Heating of oil to achieve the test temperature was accomplished indirectly with the help of refrigerated/heated circulator JULABO F25-ME and by using plate type heat exchanger. A separate electrically driven oil pump was used to circulate the heated oil through the engine head circuit. The pressure of oil can be varied by changing the speed of oil pump through ABBASC150 pump controller. 'K' type thermocouple was used to monitor the lubricant inlet temperature and displayed on the computer screen, continuously. The complete oil flow circuit in the engine valve train test rig. During the test run, constant oil supply pressure was maintained with the help of a feedback Proportional Integral Derivative (PID)

controller. The oil pressure was monitored with the help of a Piezo-resistive pressure transducer and displayed on the computer screen. The same was also used as a feedback signal to the oil pump motor for maintaining steady inlet oil pressure. An analogue pressure gauge was also installed in the test rig to monitor the oil pressure entering the engine head. Proper shielded cables and electrical earth was ensured in the test rig to avoid any electrical noise and also to protect the equipment. Insulation of all the oil pipes was carried out to reduce heat loss.

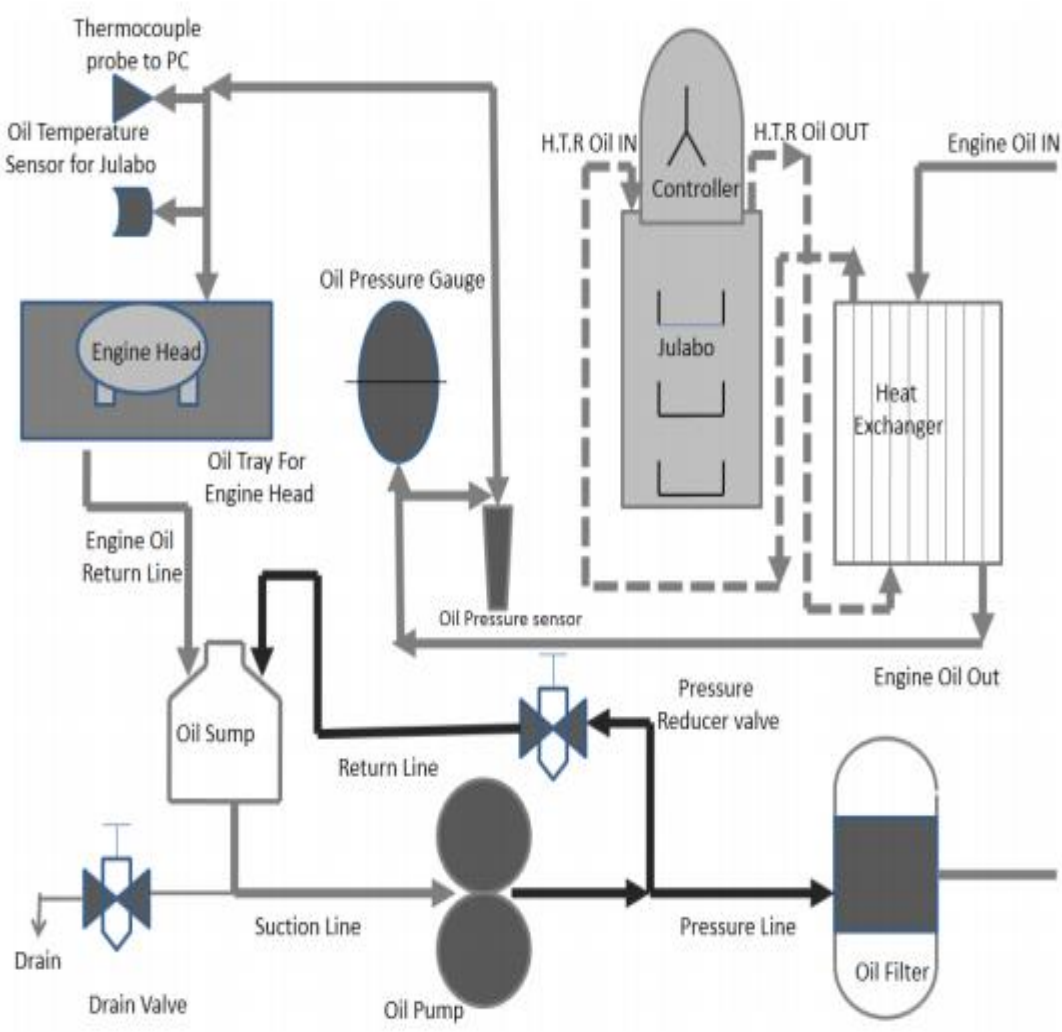

Figure 3.3: Complete oil flow circuit of the engine valve train test rig

Test Rig Sensors Wiring Diagram and LABVIEW Program

Thermocouple:

Follow these steps to connect thermocouple to NI-9219

- Identify positive and negative terminal of k-type thermocouple
- Open LabVIEW Daq assistant, select channel to use, click next then at top of window click wiring diagram and connect thermocouple to NI card as per diagram
- Set built-in cold junction compensation
- Green wire +ve, white wire -ve terminal

LabVIEW Vi for Thermocouple and Wiring Diagram

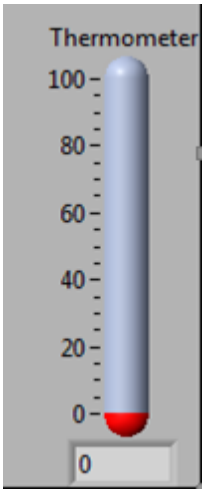

Figure 3.5: Front panel

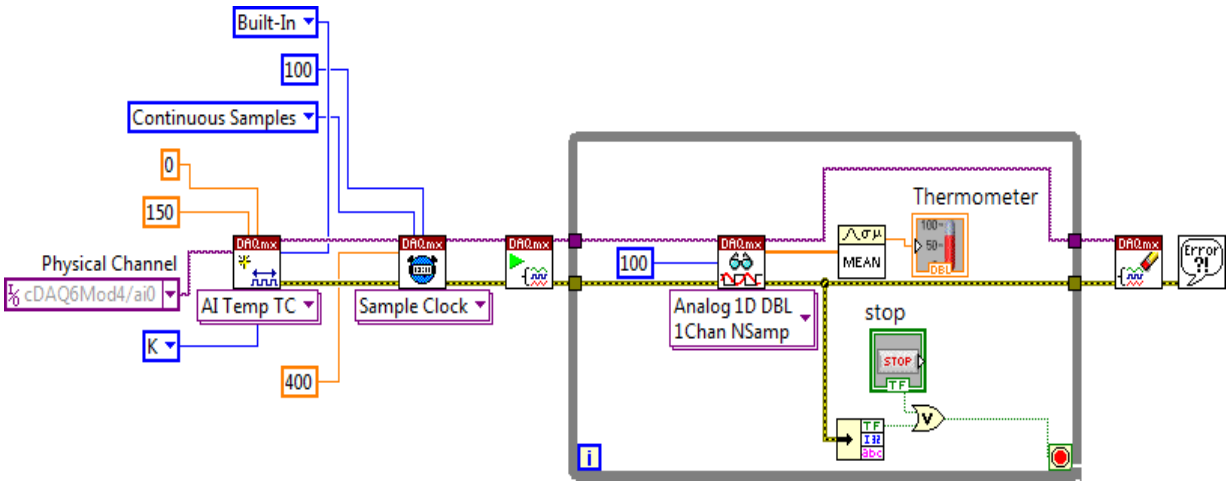

Figure 3.4: Thermocouple Block Diagram

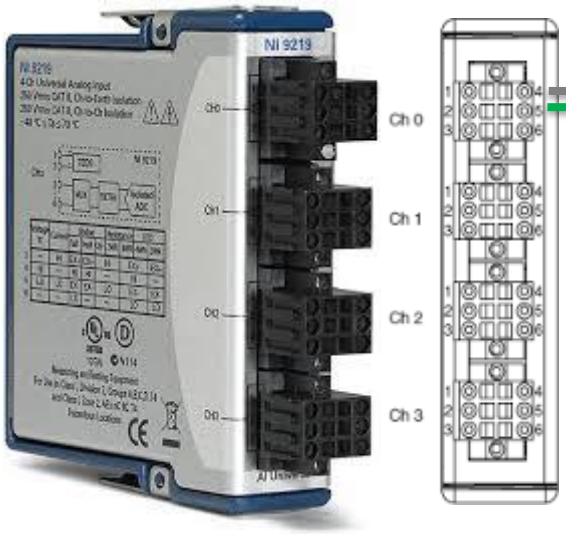

Figure 3.7: NI 9219

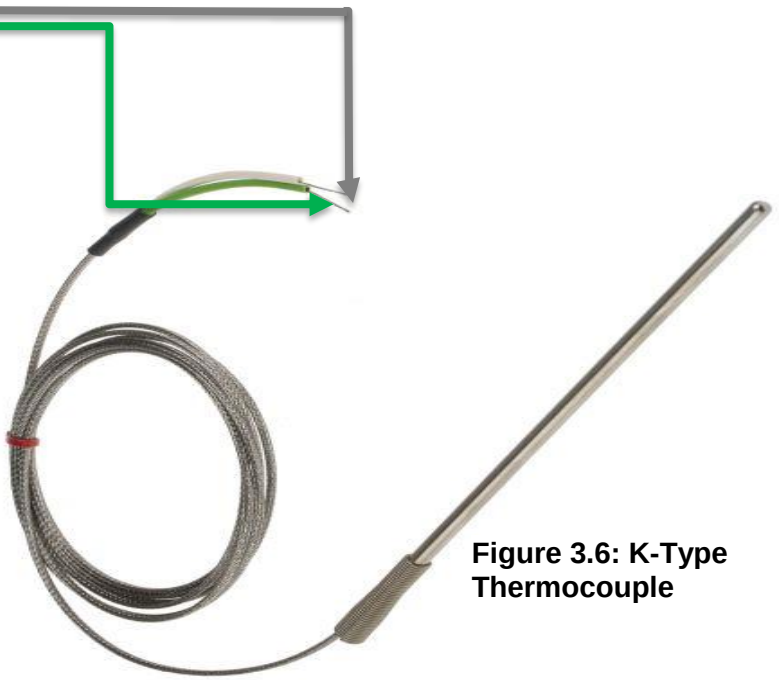

Figure 3.6: K-Type Thermocouple

Encoder

Follow these steps to connect Encoder to NI-9401

- Use only five-volt Dc supply for external Voltage excitation because NI-9401 may burnt if signal voltage exceeds 5volts.Further go through NI-9401 data sheet
- If you are using for example 12volts Dc supply, convert into 5volts by using any Voltage divider method
- Preferable to use Z-Channel signal for speed measurement because it prone to less noise.
- Open daq-assistant select ctr terminal, next window you have signal name PFI 0 etc. which represent at which terminal of NI-9401 you have to connect encoder wire.
- Open NI-9401 pinout from google to find its terminal names

LabVIEW Vi for Encoder and Wiring Diagram

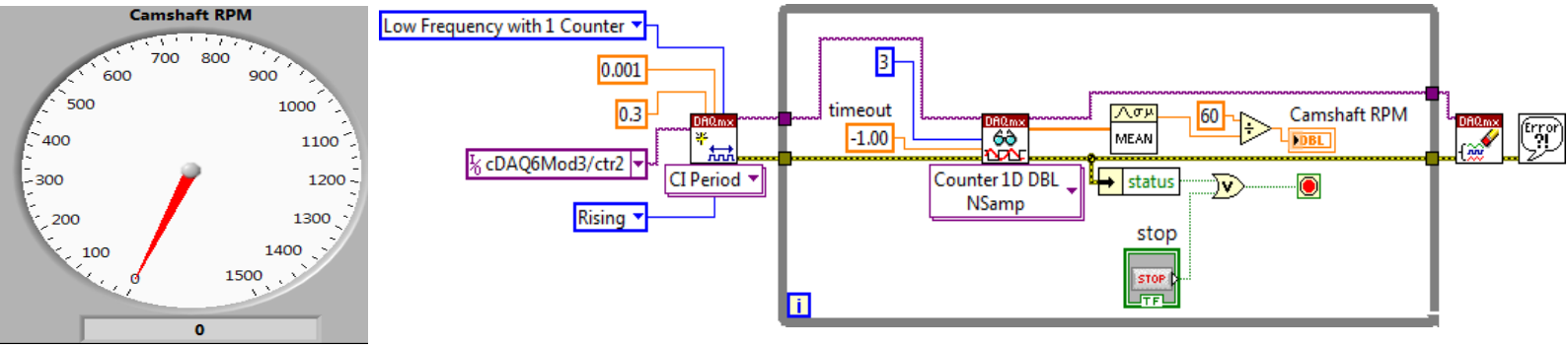

Figure 3.9: Encoder Vi Front Panel and Block Diagram

Figure 3.8: Dc Supply

Encoder Wires
+Vcc (white wire)
0V (black wire)
Z-Channel (orange)

Figure 3.11: Encoder Pinout

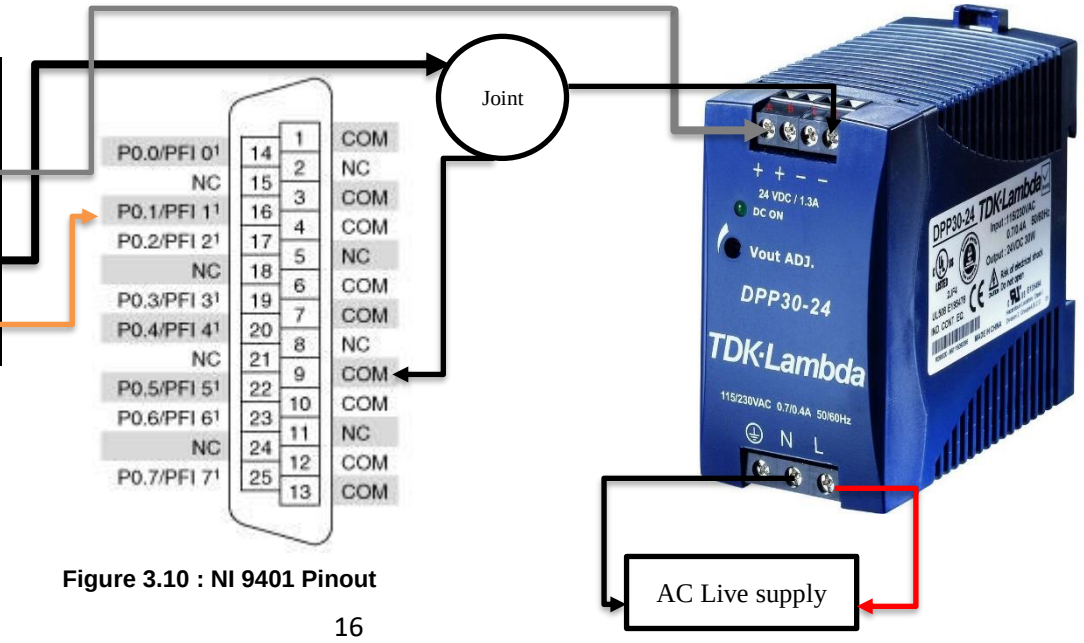

Figure 3.10 : NI 9401 Pinout

Pressure Sensor

Follow these steps to connect Pressure Sensor to NI-9215

- Find Pressure sensor wires terminal name
- Check NI-9215 pinouts
- Open daq-assistant select AI terminal, next window you have signal name AI 0 etc. which represent at which terminal of NI-9215 you have to connect Pressure sensor wire.
- Pressure sensor data sheet shows it is 0-6 bar at 0-5volts. Which means 1bar is equal to 0. 833volts. Map this value in LabVIEW Vi
- External Excitation voltage is 12volt Dc supply

LabVIEW Vi for Pressure Sensor and Wiring Diagram

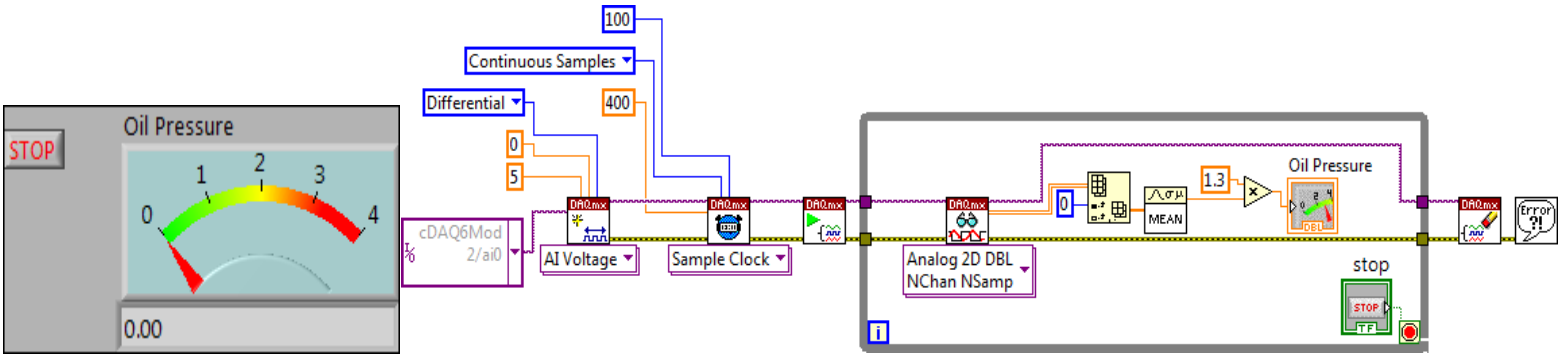

Figure 12: Pressure Sensor Vi Front Panel and Block Diagram

Pressure Sensor wire terminals
0V (blue wire)
+Vcc (Red wire)
Signal (Green wire)

Figure 13: Pressure sensor Pinout

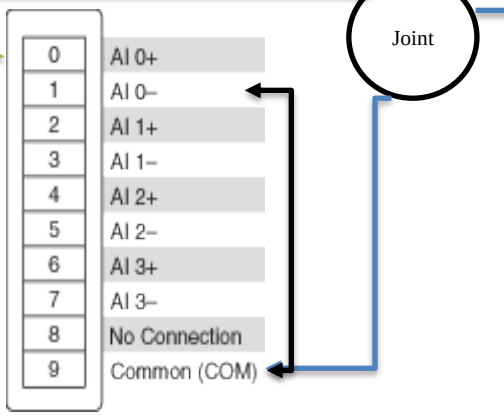

Figure 14:NI 9215 Pinout

Figure 15: Dc Supply

Cam Shaft Variable Frequency Drive Wiring

Parker VFD wiring with Daq Cards

We have used Parker VFD to control cam shaft motor speed alone with PID feedback

Macro 3: PID

PID error derived from the difference of 2 analog inputs.

Digital input to disable PID.

Additional Operator Menu display parameters.

Control Wiring I/O			
Terminal	**Name**	**Purpose**	**Comment**
2	ANALOG INPUT 1	Process Setpoint	0V = 0%, 10V = 100%
3	ANALOG INPUT 2	Process Setpoint Trim	0V = 0%, 10V = 100%
6	ANALOG OUTPUT 1	Ramp Output	absolute speed demand 0V = 0%, 10V = 100%
12	DIGITAL INPUT 1	Run Forward	24V = run forward
13	DIGITAL INPUT 2	Run Reverse	24V = run reverse
14	DIGITAL INPUT 3	Not Stop	24V = RUN FWD and RUN REV signals latched 0V = RUN FWD and RUN REV signals not latched
15	DIGITAL INPUT 4	Remote Reverse	0V = remote forward 24V = remote reverse
16	DIGITAL INPUT 5	Jog	24V = jog
17	DIGITAL INPUT 6	PID Enable	24V = PID enable
18	DIGITAL INPUT 7	Remote Trip Reset	24V = reset trips
19	DIGITAL INPUT 8	External Trip	Non-configurable 0V = Trip (connect to terminal 20)
21, 22	DIGITAL OUTPUT 1	Health	0V = tripped, i.e. not healthy
23, 24	DIGITAL OUTPUT 2	Running	0V = stopped, 24V = running
20	24 volts	24volt	24 Volt
1	0 volt	0 Volt	0 Volt

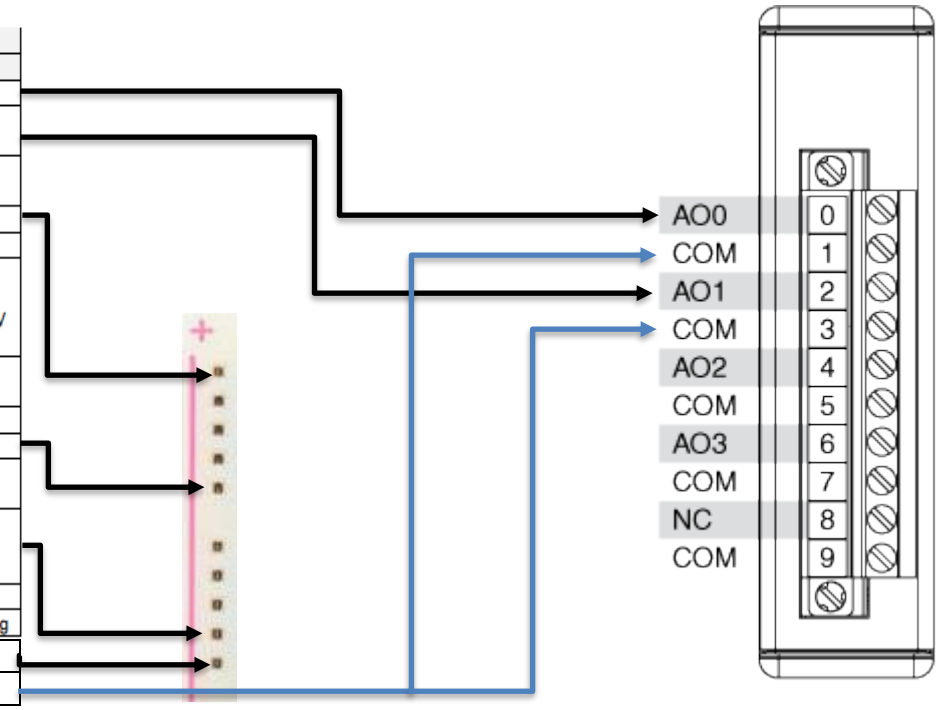

Figure 3.16: Parker VFD drive Pinouts

Figure 17:NI 9263 Pinout

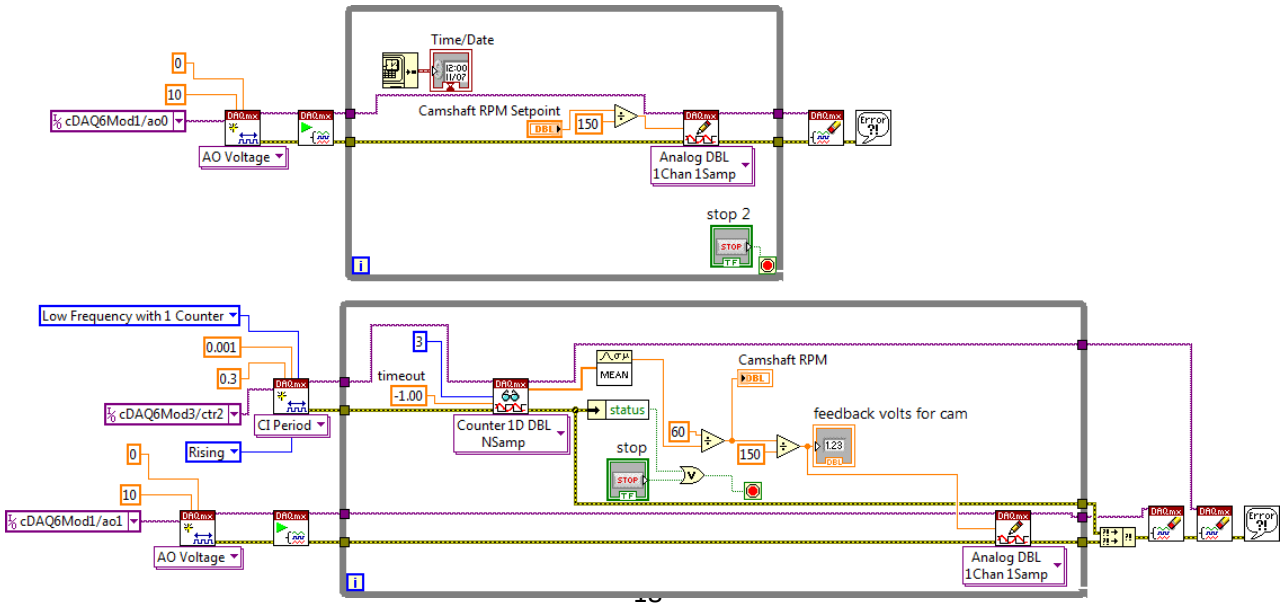

Figure 3.18: Complete Block Diagram for PID feedback Cam Shaft Motor control

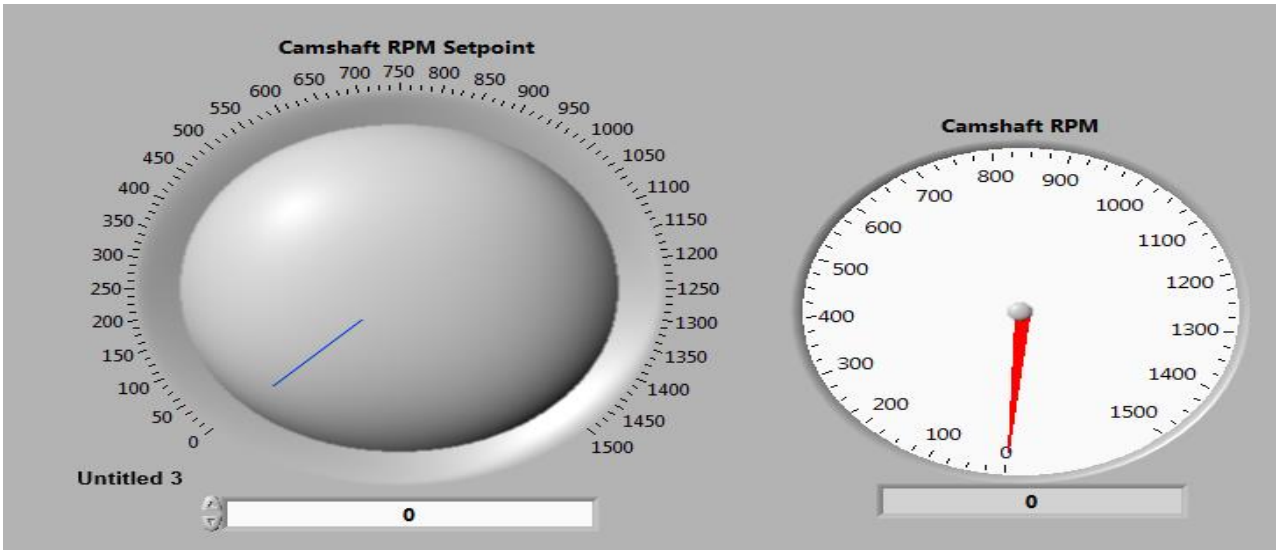

Figure 3.19: Complete Block Diagram for PID feedback Cam Shaft Motor control

Steps to understand Figure 3.19 to 3.21

- 1v = 150 rpm, 2v = 300 rpm, 10v = 1500rpm
- AO of NI 9263 connect with VFD AI which means if you generate one volt from LabVIEW, this one volt generated by NI 9263, receive at VFD AI. In return VFD drives motor at 150 rpm. In short you are running motor Via LabVIEW.
- AO 0 is connected to AI 1, give value of RPM to VFD at which you wish to drive motor. For example, if you set 300rpm from front panel. LabVIEW generates 2volt signal at VFD.
- VFD has built in PID control application so select macro 3 application for PID. After selecting Marco 3 you need to do addition changings in VFD settings. So, I have made new application macro named as PID==SOBANSAIR. Just Restore this macro in VFD you don't need to tangle in VFD settings
- AO 1 is connected to AI 2, gives feedback signal to VFD.
- Encoder measures real time camshaft speed and then this signal is fed into VFD by NI 9263. So that setpoint RPM can be compared with Actual RPM in VFD. So that camshaft always run at setpoint RPM value.
- Connect encoder to Daq card as shown in encoder wiring.

Cam Shaft Variable Frequency Drive Wiring

Parker VFD wiring with Daq Cards

We have used ABB VFD to control Oil pump motor alone with PID feedback

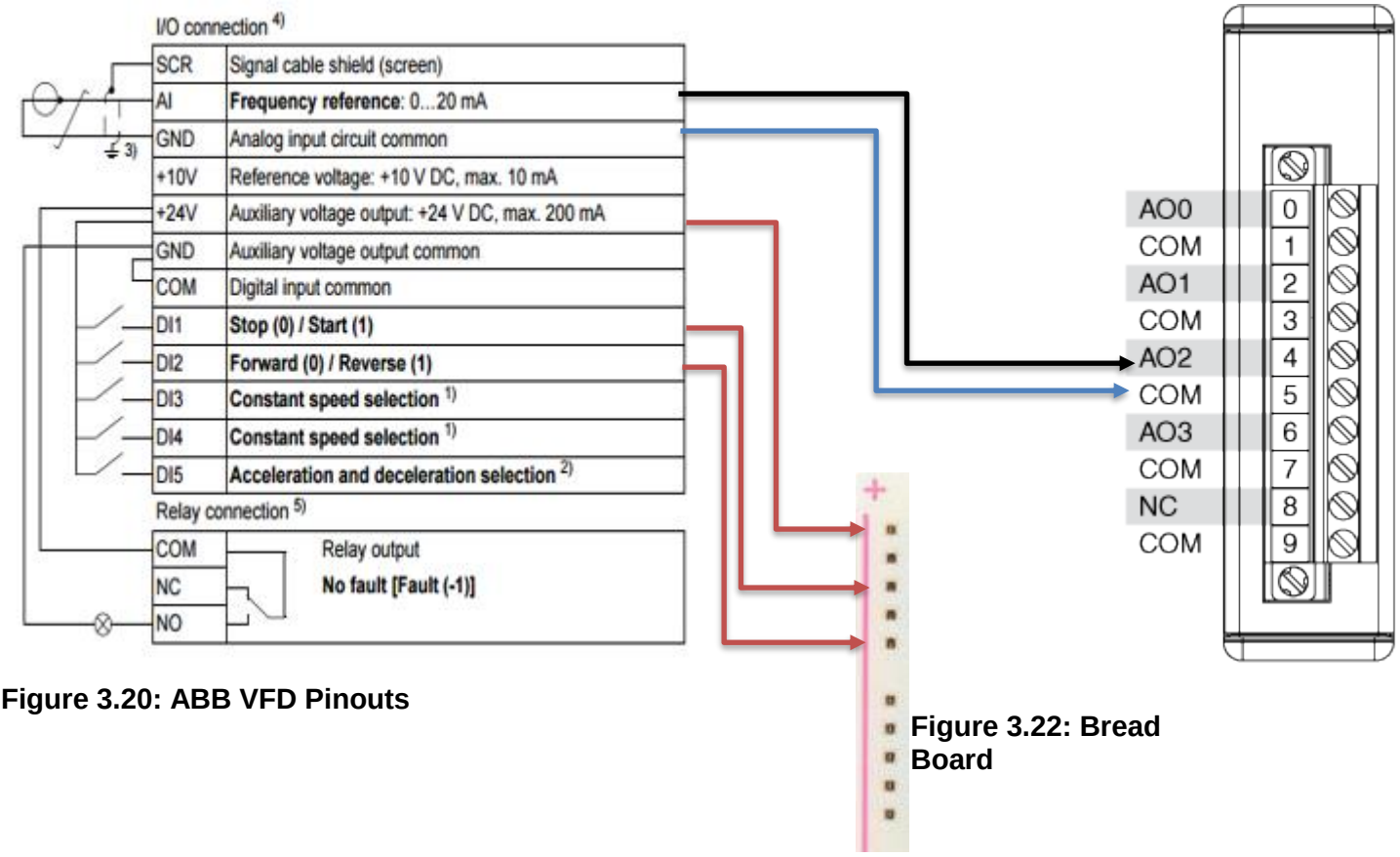

Figure 3.20: ABB VFD Pinouts

Figure 3.22: Bread Board

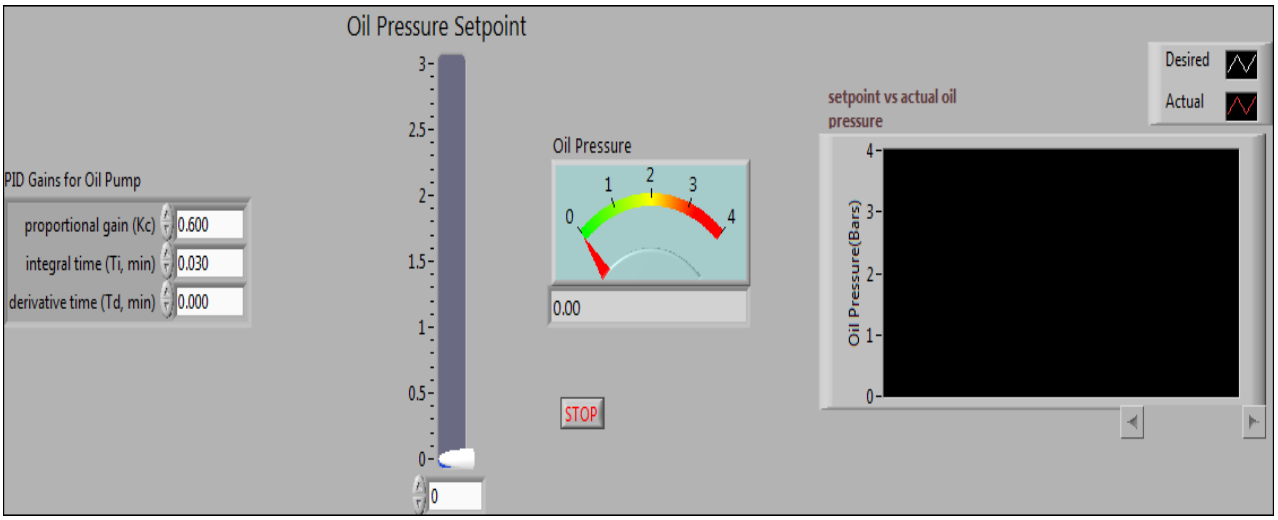

Figure 21: Front Panel of PID Feedback based Oil Pump Motor Control

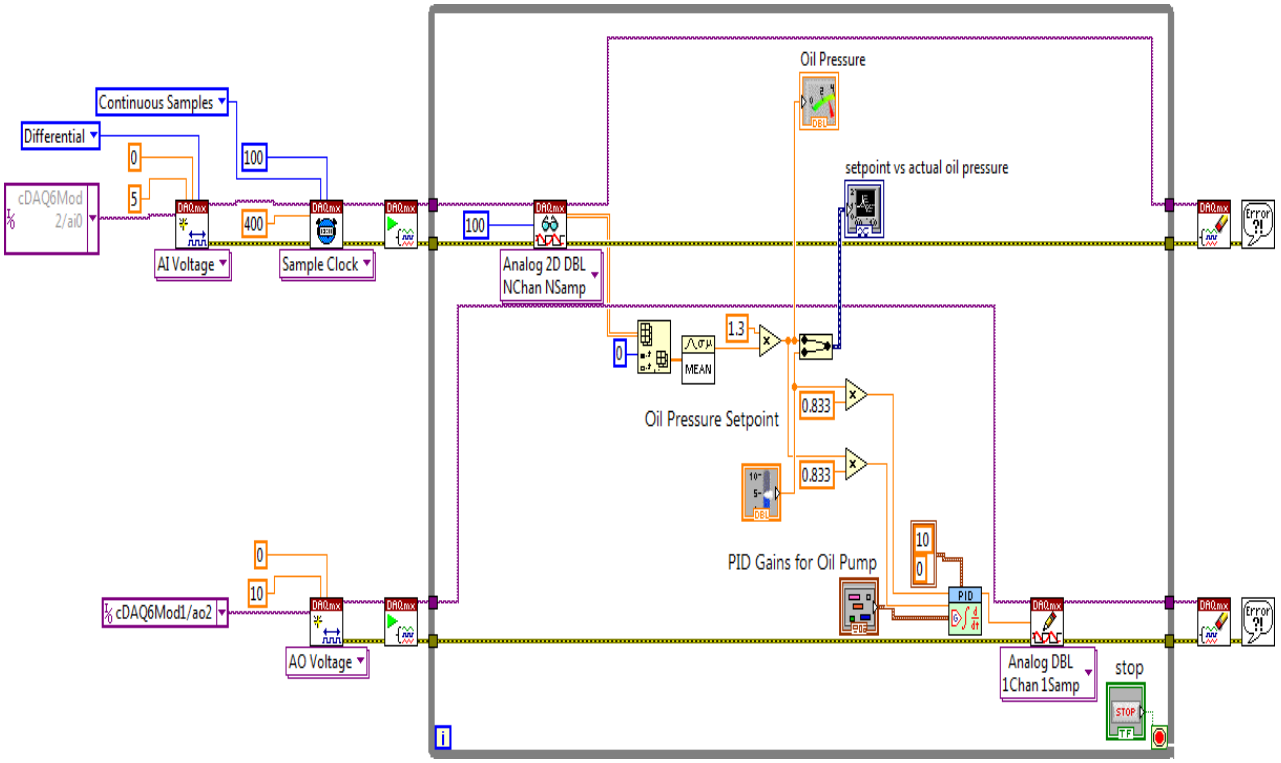

Figure 3.23: Front Panel of PID Feedback based Oil Pump Motor Control

Steps to understand Figure 3.22 to 3.25

- 1bar = 0.833 volt, 2bar = 1.666 volts. Mapping is done in LabVIEW code
- Connect pressure senor to DAQ card as described
- We have used LabVIEW built in PID option.
- In this case, setpoint pressure and actual pressure are feed into PID icon in LabVIEW so that only that voltage value fed into ABB VFD that correspond to desired oil pressure.
- AO 2 is connected to ABB VFD AI 1
- VFD has its built-in PID application macro. To understand it go through manual.

Complete Engine Head Test Rig:

- Combine all LabVIEW Vi's into single Vi so that you can control Engine Head Test Rig by one LabVIEW Vi.
- Combine all wiring diagrams as described above

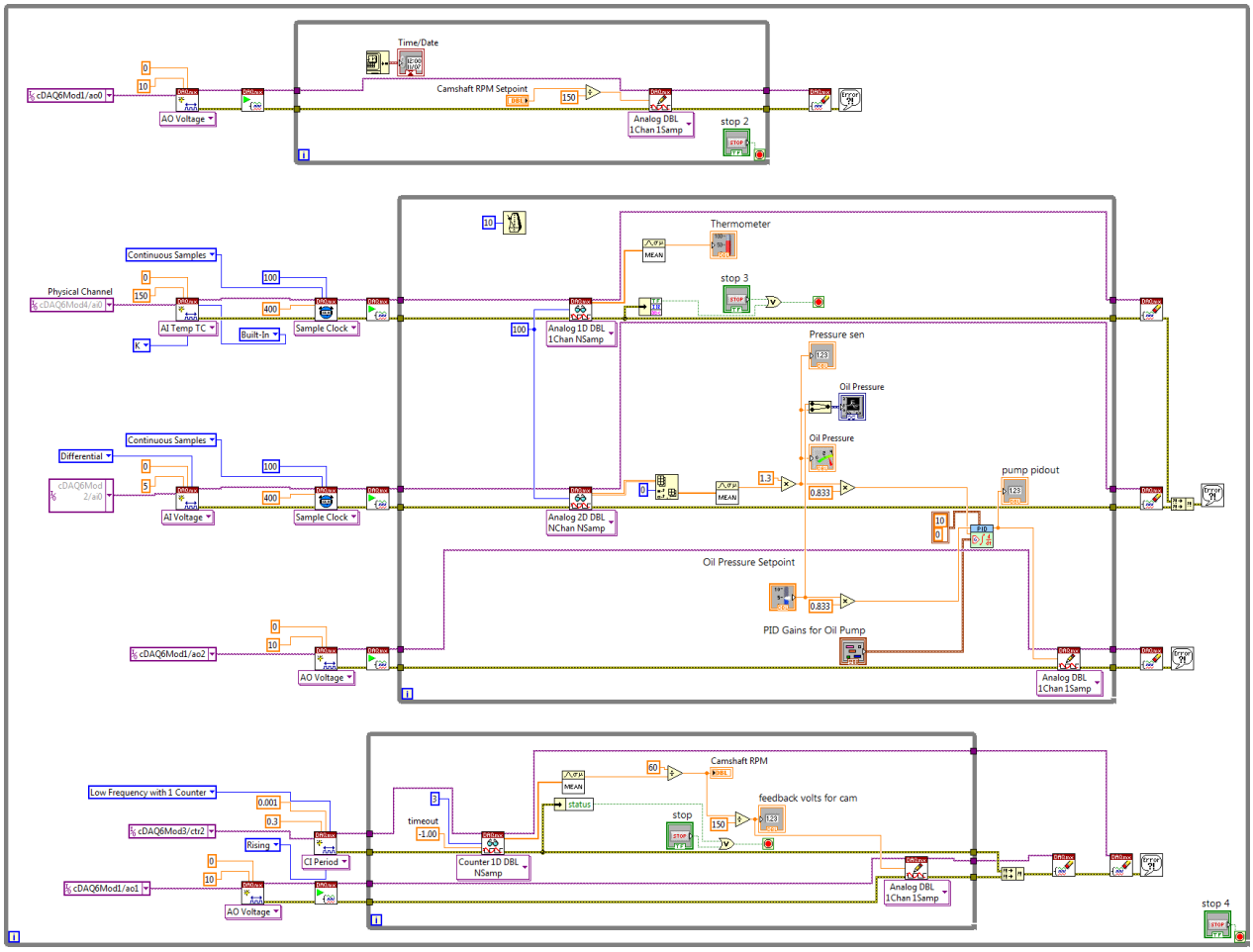

Figure 3.26: Block Diagram of Engine Head Rig

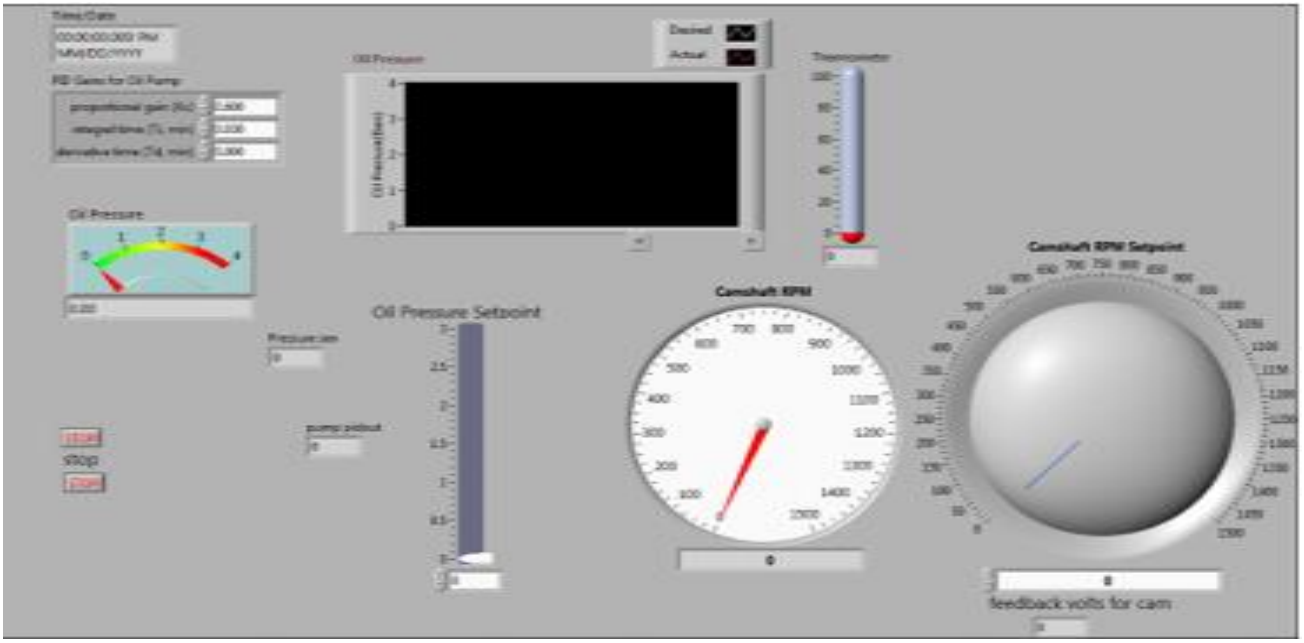

Figure 3.27: Front Panel of Engine Head Rig

CHAPTER 4: METHODOLOGY

Selection of Sensor

First Approach: TMR Sensor

Tunnel Magneto Resistive (TMR) sensors are highly stable, epoch-making magnetic sensors that achieve high output, high accuracy, and less temperature drift and aging deterioration versus GMR sensors. Thanks to their high measurement sensitivity, combined with high output voltage and angle measurement accuracy, TMR sensors give developers significantly higher degrees of flexibility for their design work.

TMR sensors however were not used in the thesis because they are monopolar, meaning a monolith magnet would have to be mounted on the roller. This was not possible since such a large change would significantly alter the roller and thus temper with the collected results. We needed an approach that would require minimal interference with our system due to which the use of TMR sensors was foregone.

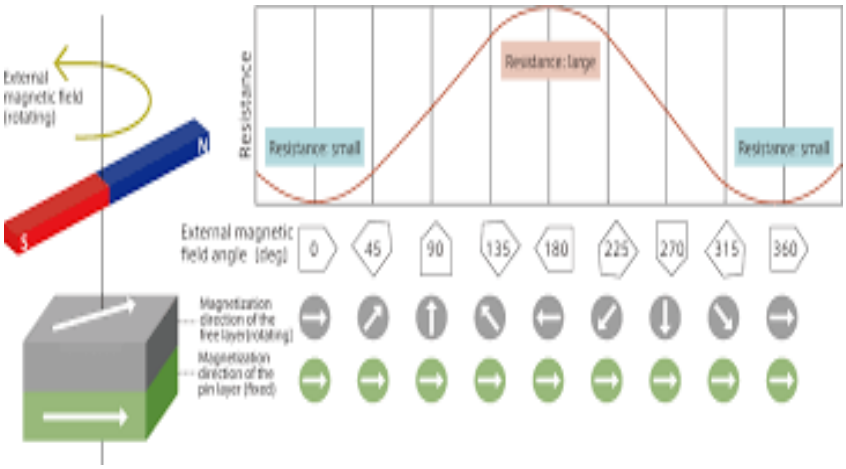

Figure 4.1: Working of TMR Sensor

Second Approach: TMR Sensor

Giant Magneto-resistive sensors (GMR) are magnetic switches manufactured by NVE Corporation. These sensors work on the principle of Giant Magneto resistance meaning, when the magnetic field is applied to the GMR sensor, it gives a logical high signal and when the field is removed output signal dies out. The ideal magnetic response is shown in the figure below:

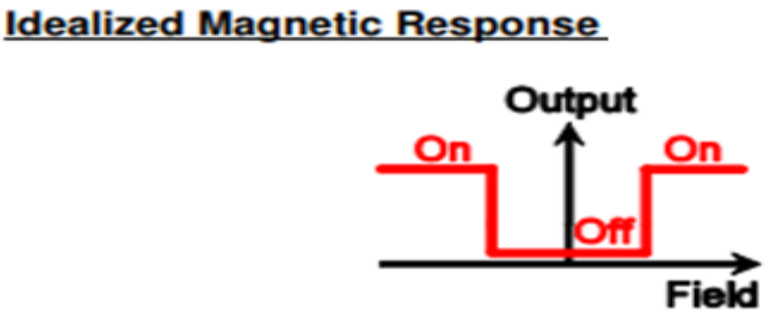

Figure 4.2: Idealized Magnetic Response of GMR sensor

Multiple variations of the GMR sensors were available to us as shown in the below mentioned figure. The sensors were divided based on their threshold magnetic field required for actuation, the chip size and the duty cycle. Since we were working with fast spinning objects i.e. with a frequency of the range of 1000 Hz, we had to utilize a continuous duty cycle. Moreover, the magnets that were used were powerful and in order to ensure magnetic interference did not disrupt the sensor signal we used a threshold of 28 Oe. Finally, since as mentioned before, limited space was available for instrumentation, we utilized the smallest sensor available i.e. the 1.1x1.1 mm sensor.

Part Numbering

The following example shows the ADL-Series part-numbering system:

ADL 0 21 - 14E

Base Part
ADL = 2.4 – 3.6 V
Nanopower digital switch

Duty Cycling
0 = 55 Hz typical
1 = 30 Hz typical
9 = Continuous duty

Typ. Magnetic Operate Point
21 = 20 Oe
24 = 28 Oe

Package Type
14E = 1.1 mm x 1.1 mm
ULLGA (RoHS)

Available Parts

Available Part	Duty Cycled?	Update Freq. (typ.)	Operate Point (typ.)	Package	Package Marking
ADL021-14E	Y	55 Hz	20 Oe	ULLGA	V
ADL024-14E	Y	55 Hz	28 Oe	ULLGA	C
ADL121-14E	Y	30 Hz	20 Oe	ULLGA	B
ADL124-14E	Y	30 Hz	28 Oe	ULLGA	D
ADL921-14E	N	Continuous	20 Oe	ULLGA	M
ADL924-14E	N	Continuous	28 Oe	ULLGA	N

Figure 4.3: Part-Numbering of GMR Sensors

In summary we used the ADL 924-14E due to the following reasons:

1. Continuous duty cycle (ADL 9XX-XXX)
2. Precise detection of 28 Oe magnetic fields (ADL 924-XXX)
3. Ultra-miniature 1.1 x 1.1 x 0.35 mm package dealing with our tight space constraints (ADL 924-14E)
4. Low power consumption and operating voltage

The engineering drawing and pin configuration is shown below:

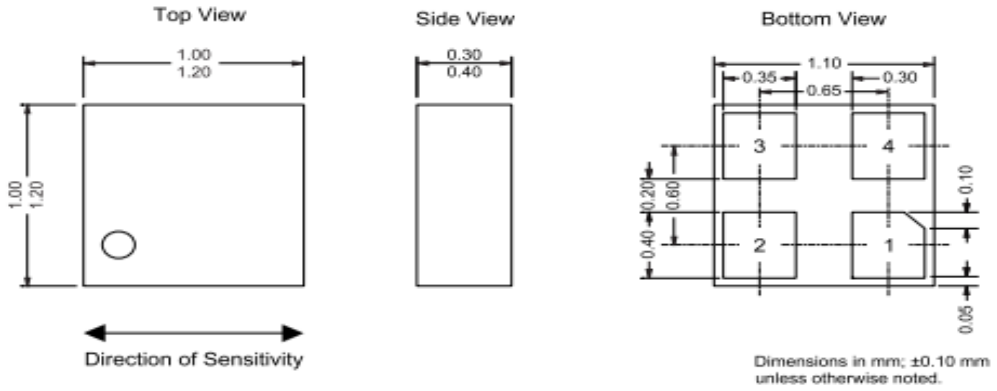

Pin 1	No Connect
Pin 2	V_{DD}
Pin 3	Out
Pin 4	Ground

Figure 4.4: Engineering Drawing and Pin Configuration of GMR Sensor

Here out of the 4 pads, only 3 pads are functional with pad 1 being a dummy pad. Pad 2 requires a 2.8V-3.6V voltage supply with pad 3 and 4 being output and ground respectively. It is also important to attach a pull-up resistor when using the sensor in the fashion shown below.

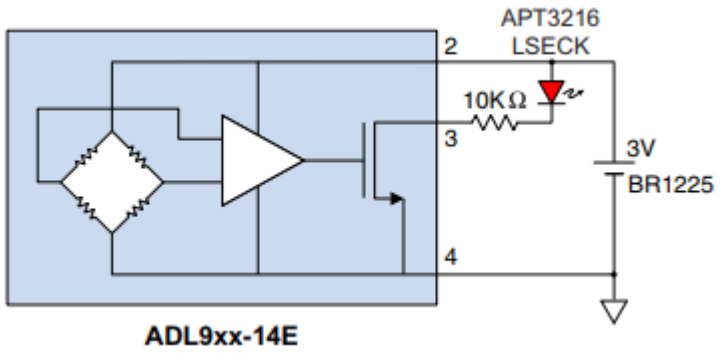

Figure 4.24: Pull Up Resistor Configuration

Since the sensor was not locally available in Pakistan, we ordered it online from LCSC, Electronic Component Distributors Company in China.

Mounting of GMR Sensor on PCB:

PCB Design

A PCB had to be designed which would accommodate 3 wires that could access the miniscule sensor yet without making the assembly too large. As our sensor was 1.1mm x 1.1mm we decided to use Teflon wires of AWG 30 meaning a wire diameter of 0.25mm only.

The basic schematic of the PCB along with the desired dimensions is shown in the figure below:

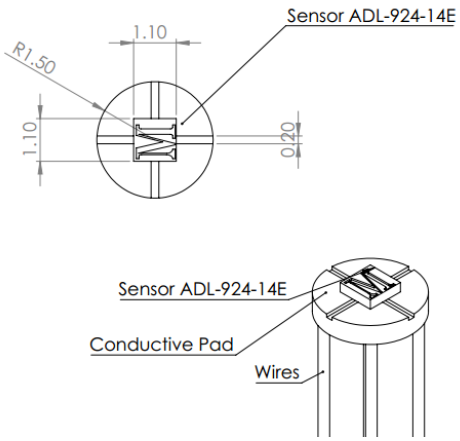

Figure 4.6: Conceptual Design of Mounted Sensor

PCB design was made using DipTrace® and the software-based schematic is shown below. A 2-layer PCB was designed, the top layer or TOP COPPER was used for the footprints of the GMR sensor and the bottom layer or BOTTOM COPPER was made to solder the wires to the PCB. The two layers were shorted using vias. This was done so that we had a large area to solder the wires in order to provide a firm grip and add to the robustness of the system without compromising on the area given to the sensor footprints.

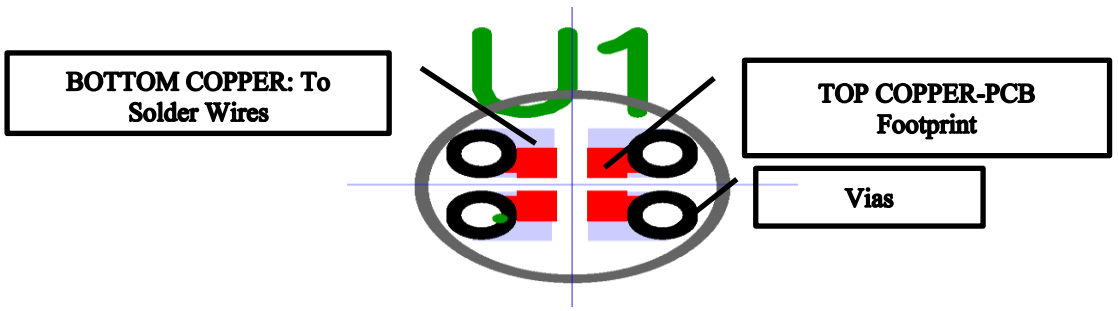

Figure 4.7: PCB Schematic

The final manufactured PCB can be seen below.

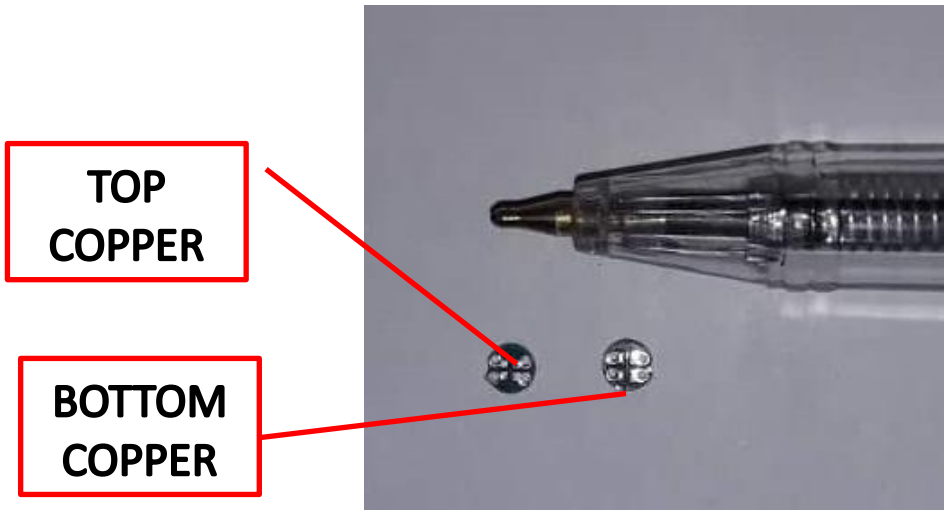

Figure 4.8: Manufactured PCB

Since cost was an important factor in this project, we explored all the possibilities for having the sensor soldered in a robust fashion. Robustness was another constraint since our sensor would experience a harsh environment with high temperatures and continuous interaction with hot lubrication oil.

Soldering

The following approaches were used to solder the GMR sensor to the designed PCB:

Manual Soldering

Soldering manually resulted in the burning out of the sensors due to very high temperatures of the soldering iron. Moreover, it resulted in large solider peaks which meant magnets would be unable to approach the sensor without touching the solder mounds first. This would result in short circuiting and could also lead to hamper the rotation of the roller if the two came into contact.

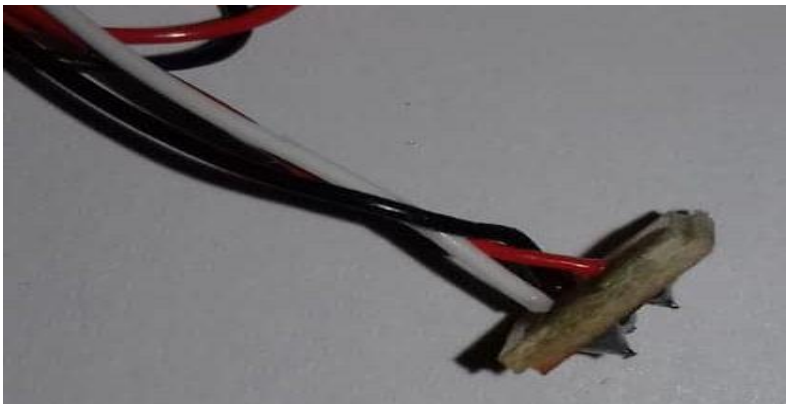

Figure 4.9: Manual Soldering

Reflow Soldering

We decided to go for reflow soldering, however the technology for reflow soldering was not available at our university. Hence, we contacted a number of third parties for the task and finally selected Taraz Technologies to get the job done. While this approach was significantly more expensive than manual soldering, it provided us with much more robustness and accuracy within the 3mm PCB board.

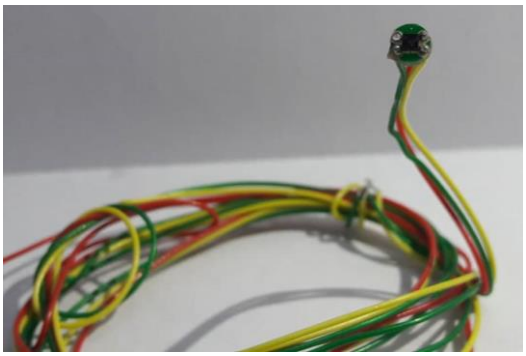

Figure 4.10: Reflow Soldered

Mounting the PCB in Follower

Once the PCB was manufactured, we had to make a suitable holder that would position the PCB rigidly in close proximity to the magnets embedded in each of the roller. Since we had two roller types (DAF Truck Tappet and Toyota Prius Finger Follower) we implemented two methods to position the sensor:

1) A customized bolt for DAF Truck Tappet Follower
2) An acrylic holder for Toyota Prius Finger Follower

1 Bolt for DAF Truck Tappet Follower

The first task was selecting a bolt size. The diameter of our PCB was 3mm which meant that the minor diameter of the bolt/screw would have to be greater than 3mm. Space was also a constraint so we could not select bolts/screws that were too large and hence we went with an M5 screw.

There were two ways to make space for wires protruding from the PCB. We could either drill a through hole or mill a slot in our screw. The latter design, i.e. a slotted bolt was not feasible as this would expose the wires making them more likely to experience damage due to which we decided to drill a through hole in the bolt.

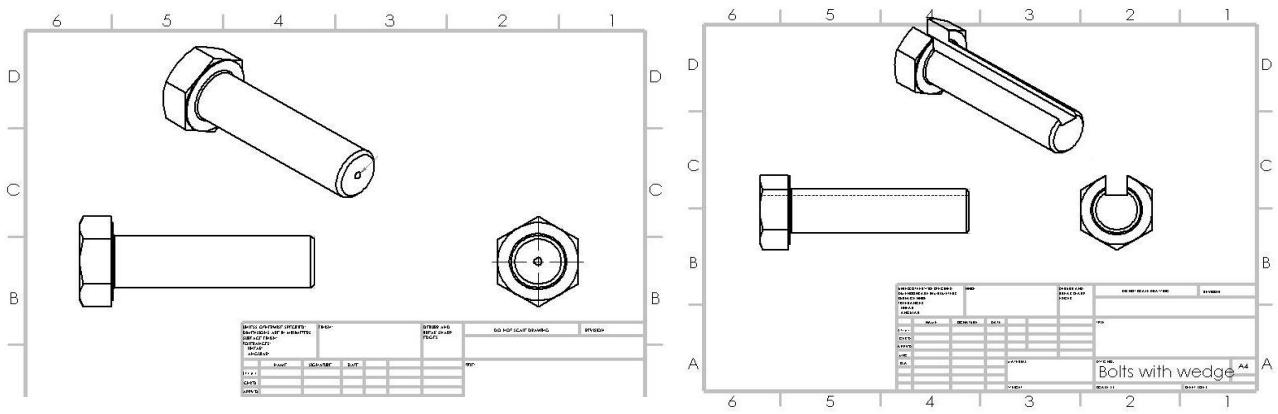

Figure 4.11: Design of Two Types of PCB Holders

The engine also had limited space which meant that a bolt/screw with a head would not work and hence we decided to use grub screws (headless screws) instead of normal screws in order to save on space. We also machined threads into the follower casing to firmly clasp the screw with the follower body to ensure the sensor position does not change due to vibrations. The final screw selected was an **M5 Grub Screw.** In order to securely position the sensor on the bolt, instead of simply drilling a through hole in the bolt, we made a step within the bolt so that the sensor had a seat on which it would firmly adhere via epoxy.

This meant that two changes had to be made to the standard M5 grub screw:

1) Machine a seat for the PCB
2) Provide space for wires to protrude from opposite end

The following design was finalized.

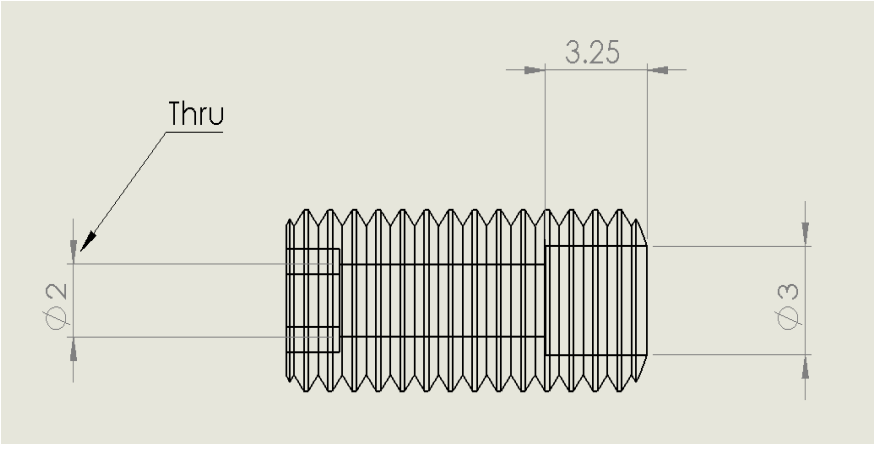

Figure 4.12: Final Design of PCB Holder for DAF Follower

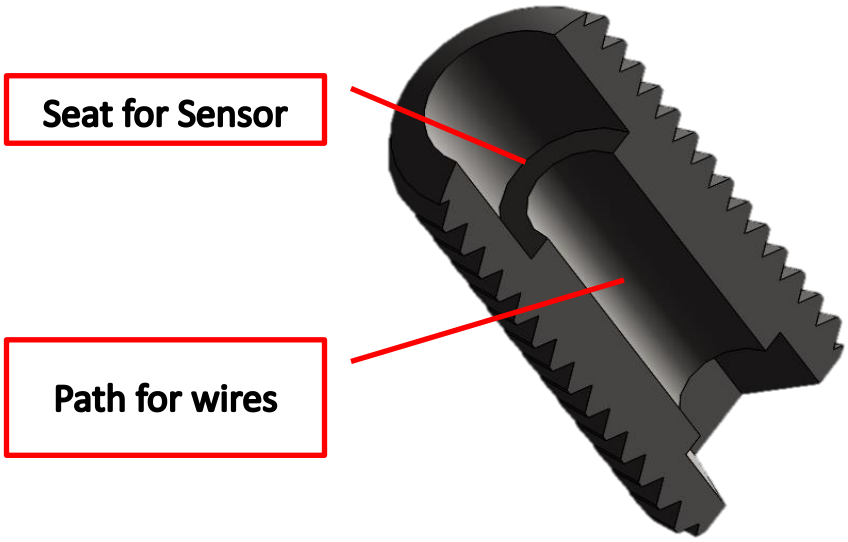

Figure 4.13: 3D Model of PCB Holder for DAF Follower

Once the bolt had been machined, the PCB was inserted, and the top was sealed using epoxy to secure the PCB.

The final bolt is presented below:

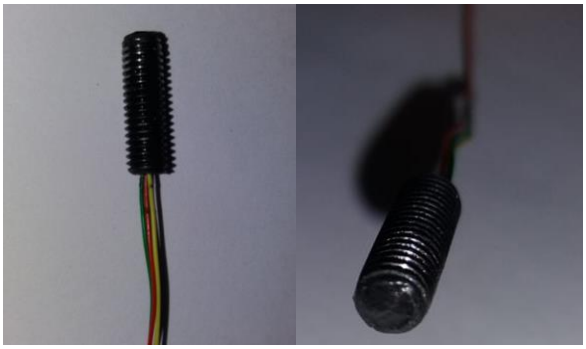

Figure 4.14: Sensor-Mount Assembly

Acrylic Sensor Holder for Toyota Prius Roller

The aforementioned sensor holding method could be used in the DAF Follower due to the follower's large size. The Toyota Prius follower on the other hand had even more stringent space restrictions and the largest hole we could drill in the casing was of 4mm. This meant that we could not incorporate a removeable sensor holder in the follower and would instead have to fix it permanently on the roller casing while ensuring that the PCB does not come into contact with any

of the surrounding metal surfaces which might cause it to short circuit. The following casing was finalized and manufactured:

One end of the holder was closed in order to ensure that the sensor does not come into contact with the rotating roller which the other end was opened to allow the passing of the wires.

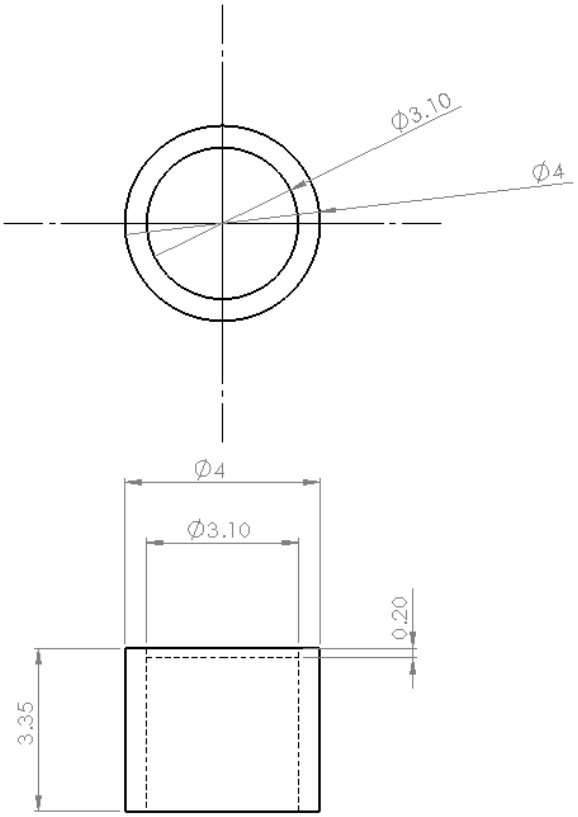

Figure 4.15: Engineering Drawing of PCB Holder for Toyota Prius Follower

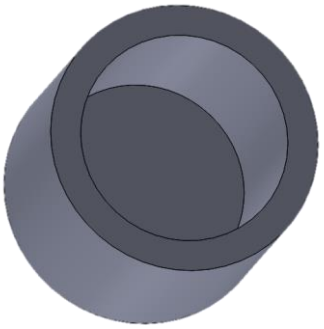

Figure 4.16: 3D Model of PCB Holder for Toyota Prius Follower

Figure 4.125: Manufactured PCB Holder for Toyota Prius Follower

AlNiCo Magnets:

As mentioned, the roller had to be instrumented in such a way that it would be divided into equal parts. This could be done by embedding the roller with 1x1mm magnets (AlNiCo) at a certain equal distance. It was necessary for these magnets to be very small due to the space constraints of the followers.

Using this method each portion of the roller would have its own magnet which would tell the sensor that a certain portion of the roller had rotated past it. Optimum spacing between magnets had to be calculated after testing on a steel strip for all the roller followers.

Figure 4.18: AlNiCo Magnet

To insert magnets in the roller we drilled holes of 1mm diameter and 1mm depths and press fitted the magnets.

These magnets would now allow us to check the slippage/inertial movements' up to a certain degree of resolution. For example, if we embedded a total of 20 magnets in a roller, that would allow us to study the effects up to a resolution of $360/20=18^{o}$.

It was however, necessary to have a minimum distance between these magnets such that their magnetic fields did not interfere with one another as shown below:

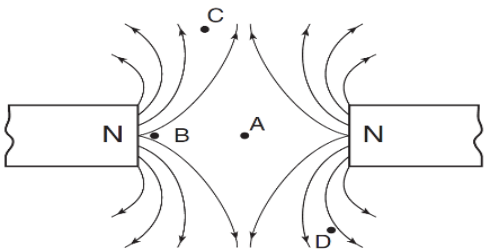

Figure 4.19: Magnetic Interference

If this happened, then the sensor would detect one magnet instead of two which would add error to our readings. Due to this, precise placement of these magnets was essential in the roller.

Selection of Magnet Spacing

Before permanent changes were made to the roller by machining, it was important to ensure that the magnets that would be placed on the roller would not interfere with each other as shown below:

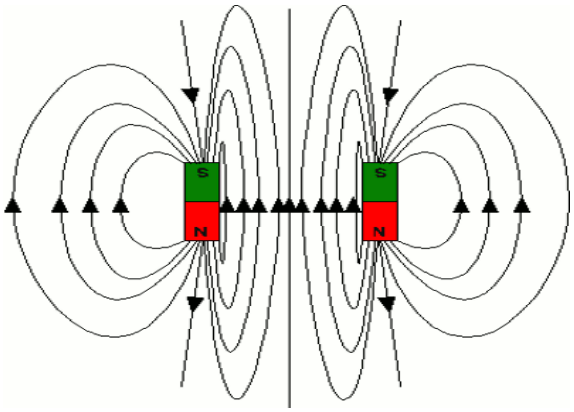

Figure 4.20: Magnetic Field

Interference of magnetic field would mean that the sensor would only be able to read one single magnet instead of two and hence instead of showing two peaks would only show one extended signal.

In order to overcome this issue, a minimum distance was to be selected. It was important that this distance would be kept as small as possible so that the number of magnets on the roller would increase which would allow us to increase the resolution of our instrumentation. A mild steel plate

was drilled multiple arrays of 4 holes each with a center to center distance of 0.5mm more than the previous one, starting from 2mm as shown.

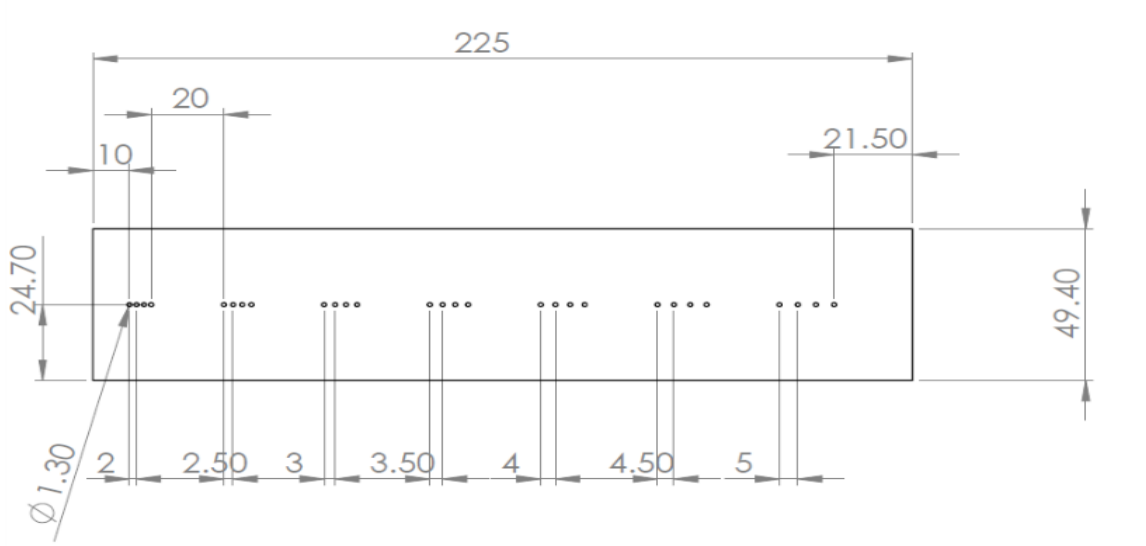

Figure 4.21: Drawing of Magnet Spacing Determination Board (dimensions in mm)

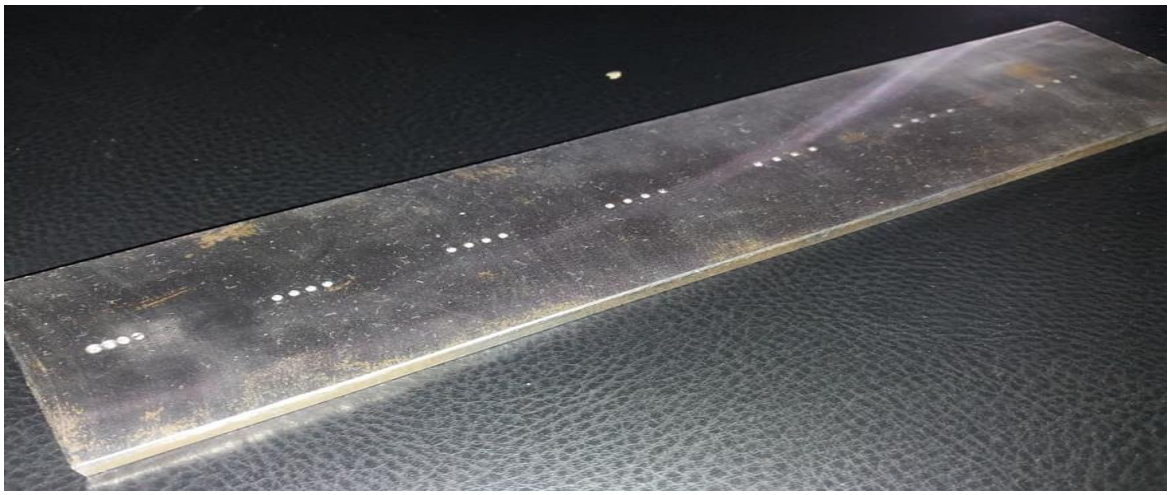

Figure 4.22: Magnet Spacing Determination Board

The AlNiCo magnets were placed in these holes and a sensor was passed over one array of holes which were at a specific center to center distance. We checked whether we would get 4 separate peaks since less than 4 peaks would mean that the sensor was missing out some of the magnets due to magnetic interference. Peaks overlapped at up to a center to center distance of 3.5mm, however, to ensure accuracy we decided on having a center to center distance of no less than 4.5mm.

Selection of Distance Between Magnet and Sensor

In order to determine the farthest distance, the sensor could be kept while still able to detect all the peaks the following set up was made.

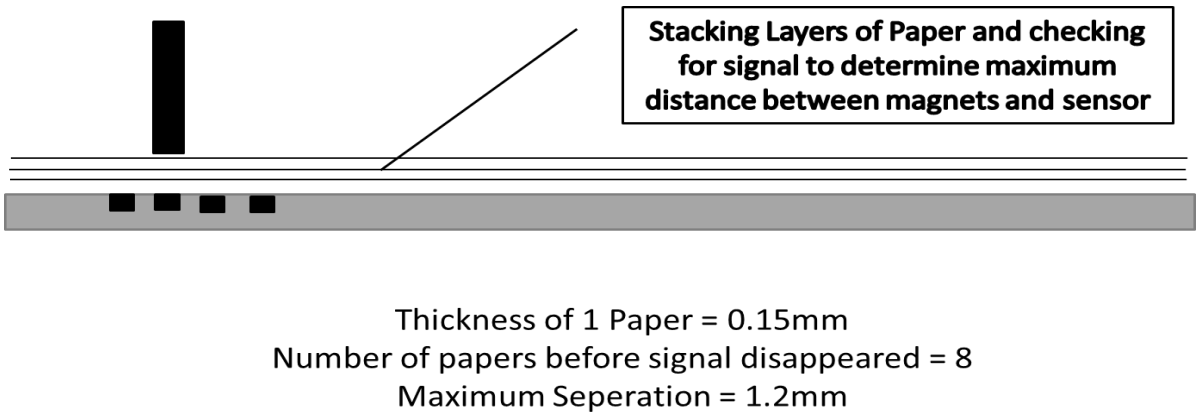

Figure 4.23: Determining Maximum Distance Between Magnets and Sensor

Stacks of papers were placed on top of each other and the sensor was passed over the papers to check if distinct peaks were being detected. Each paper was 0.15mm thick and we observed that after placing 8 papers, we started to lose the signal meaning after a total distance of 1.2mm the sensor would not be accurate. This meant that in all assemblies, the tip of our sensor had to be less than 1.2mm away from the embedded magnets on the rollers.

Magnet Positioning on DAF Truck Tappet Follower

The next task was to decide the circumferential distance for the DAF Truck Tappet Follower, where these holes would be drilled for magnet placement. The limits for this was less than 30mm diameter since that was the point where the fillet ended hence the drill at the point would not be able to grab the magnet firmly. The farther we shift the circumference on which we would drill the holes the more magnets we could accommodate on one side of the roller.

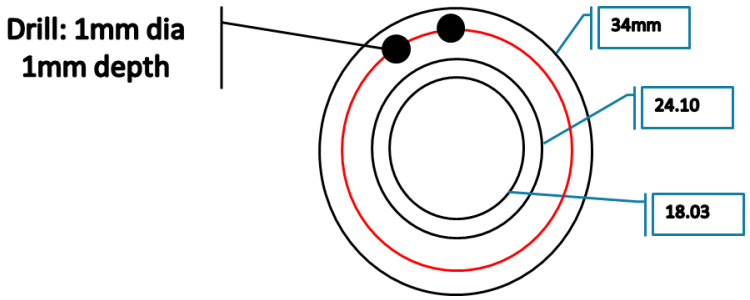

Figure 4.24: Magnet Placement on DAF Tappet Follower

This was dictated by the following formula subjected to the below mentioned constraints

$$Number\ of\ Magnets = \frac{\pi \times Diameter\ of\ Drill\ Circle}{Spacing\ between\ magnets}$$

Constraints:

1. Spacing Between Magnets > 4.5mm
2. 24.10mm ≤ Diameter of Drill Circle ≤ 30mm

Based on the above-mentioned data and including tolerance factors, the table shown below was generated. We were able to drill 18 holes in the roller at a reasonable circumferential distance of 28mm while keeping the magnets at a distance of a good 5mm. This meant that each magnet would be placed 20 degrees apart from its neighboring magnet.

D hole circle (mm)	Rad hole circle (mm)	Circumference (mm)	No of Magnets with 3.5 mm gap	Angle between Magnets	No. of Magnets with 4mm gap	Angle between Magnets	No. of Magnets with 4.5mm	Angle between Magnets	No. of Magnets with 5 mm	Angle between Magnets
24.27	12.135	76.25	22	17	19	19	17	21	15	24
24.47	12.235	76.87	22	16	19	19	17	21	15	23
24.67	12.335	77.50	22	16	19	19	17	21	16	23
24.87	12.435	78.13	22	16	20	18	17	21	16	23
25.07	12.535	78.76	23	16	20	18	18	21	16	23
25.27	12.635	79.39	23	16	20	18	18	20	16	23
25.47	12.735	80.02	23	16	20	18	18	20	16	22
25.67	12.835	80.64	23	16	20	18	18	20	16	22
25.87	12.935	81.27	23	16	20	18	18	20	16	22
26.07	13.035	81.90	23	15	20	18	18	20	16	22
26.27	13.135	82.53	24	15	21	17	18	20	17	22
26.47	13.235	83.16	24	15	21	17	18	19	17	22
26.67	13.335	83.79	24	15	21	17	19	19	17	21
26.87	13.435	84.41	24	15	21	17	19	19	17	21
27.07	13.535	85.04	24	15	21	17	19	19	17	21
27.27	13.635	85.67	24	15	21	17	19	19	17	21
27.47	13.735	86.30	25	15	22	17	19	19	17	21
27.67	13.835	86.93	25	14	22	17	19	19	17	21
27.87	13.935	87.56	25	14	22	16	19	19	**18**	**21**
28.07	14.035	88.18	25	14	22	16	20	18	18	20
28.27	14.135	88.81	25	14	22	16	20	18	18	20
28.47	14.235	89.44	26	14	22	16	20	18	18	20
28.67	14.335	90.07	26	14	23	16	20	18	18	20
28.87	14.435	90.70	26	14	23	16	20	18	18	20
29.07	14.535	91.33	26	14	23	16	20	18	18	20
29.27	14.635	91.95	26	14	23	16	20	18	18	20
29.47	*14.735*	*92.58*	*26*	*14*	*23*	*16*	*21*	*17*	19	19
29.67	14.835	93.21	27	14	23	15	21	17	19	19
29.87	14.935	93.84	27	13	23	15	21	17	19	19

Table 4.1: Magnet Position Data for DAF Truck Tappet Follower

Magnet Positioning on Toyota Prius Finger Follower

A similar calculation had to be done for the Toyota Prius Follower which had the below mentioned constraints.

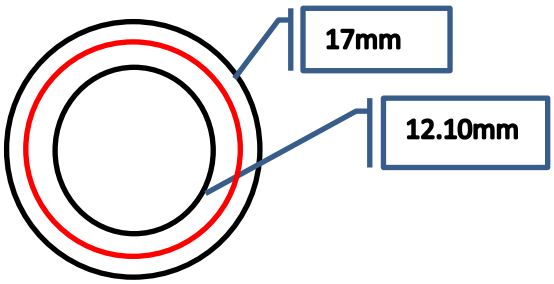

Figure 4.25: Magnet Placement on Toyota Prius Finger Follower

Constraints:

1. Spacing Between Magnets > 4.5mm
2. 12.10mm ≤ Diameter of Drill Circle ≤ 17.00mm (smaller constraint due to limited space)

Based on the above-mentioned data and including tolerance factors, the table shown below was generated.

D hole circle (mm)	Rad hole circle (mm)	Circumference (mm)	No of Magnets with 3.5 mm gap	Angle between Magnets	No. of Magnets with 4mm gap	Angle between Magnets	No. of Magnets with 4.5mm gap	Angle between Magnets	No. of Magnets with 5 mm gap	Angle between Magnets
12.7	6.35	39.90	11	32	10	36	9	41	8	45
12.8	6.4	40.21	11	31	10	36	9	40	8	45
12.9	6.45	40.53	12	31	10	36	9	40	8	44
13	6.5	40.84	12	31	10	35	9	40	8	44
13.1	6.55	41.15	12	31	10	35	9	39	8	44
13.2	6.6	41.47	12	30	10	35	9	39	8	43
13.3	6.65	41.78	12	30	10	34	9	39	8	43
13.4	6.7	42.10	12	30	11	34	9	38	8	43
13.5	6.75	42.41	12	30	11	34	9	38	8	42
13.6	6.8	42.73	12	29	11	34	9	38	9	42
13.7	6.85	43.04	12	29	11	33	10	38	9	42
13.8	6.9	43.35	12	29	11	33	10	37	9	42
13.9	6.95	43.67	12	29	11	33	10	37	9	41
14	7	43.98	13	29	11	33	10	37	9	41
14.1	7.05	44.30	13	28	11	33	10	37	9	41
14.2	7.1	44.61	13	28	11	32	10	36	9	40
14.3	7.15	44.92	13	28	11	32	10	36	9	40
14.4	7.2	45.24	13	28	11	32	10	36	9	40
14.5	7.25	45.55	13	28	11	32	10	36	9	40
14.6	7.3	45.87	13	27	11	31	10	35	9	39
14.7	7.35	46.18	13	27	12	31	10	35	9	39
14.8	7.4	46.50	13	27	12	31	10	35	9	39
14.9	7.45	46.81	13	27	12	31	10	35	9	38
15	7.5	47.12	13	27	12	31	10	34	9	38
15.1	7.55	47.44	14	27	12	30	11	34	9	38
15.2	7.6	47.75	14	26	12	30	11	34	10	38
15.3	7.65	48.07	14	26	12	30	11	34	10	37
15.4	7.7	48.38	14	26	12	30	11	33	10	37
15.5	7.75	48.69	14	26	12	30	11	33	10	37
15.6	7.8	49.01	14	26	12	29	11	33	10	37
15.7	7.85	49.32	14	26	12	29	11	33	10	36
15.8	7.9	49.64	14	25	12	29	11	33	10	36
15.9	7.95	49.95	14	25	12	29	11	32	10	36
16	8	50.27	14	25	13	29	11	32	10	36
16.1	8.05	50.58	14	25	13	28	11	32	10	36
16.2	8.1	50.89	15	25	13	28	11	32	10	35
16.3	8.15	51.21	15	25	13	28	11	32	10	35

Table 4.2: Magnet Position Data for Toyota Prius Finger Follower

According to this table, we see that even if we wish to shift the circumferential distance, we will not be able to make significant changes due to the small size of the roller. Due to this constraint we selected the middle of the roller i.e. 14.6mm placing 10 magnets per side with an angular spacing of 36 degrees to keep a distance of 4.5mm between magnets.

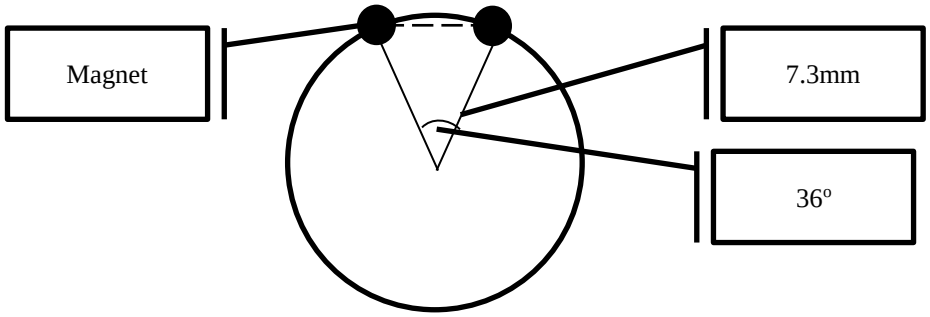

Figure 4.26: Calculation for Spacing Between Magnets

$$Magnet\ spacing = \sqrt{7.3^2 + 7.3^2 - 2(7.3)(7.3)\cos(36)} = 4.51mm$$

Furthermore, since 10 magnets would give us a small resolution, we decided to place 10 magnets on the other side of the roller as well but at an offset of 90 degrees so that we would now have a total of 20 magnets on the roller. The final roller schematic is as below:

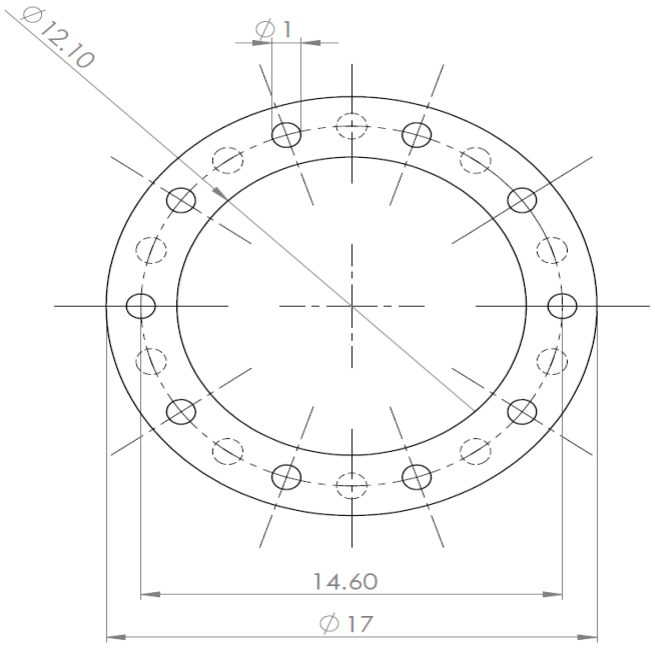

Figure 4.27: Magnet Positions on Toyota Prius Finger Follower (dimensions in mm)

Machining the DAF Roller

For the DAF Truck Tappet Follower, we had to drill holes on a circle of circumference of 28mm with 18 magnets each magnet 20^{o} apart. A CNC machine was used to drill the holes at a depth of 1.05mm. Once these holes we drilled, the AlNiCo magnets were placed in the holes and a layer of epoxy was coated on the rollers to ensure that the magnets did not bounce out of their positions due to vibrational effects.

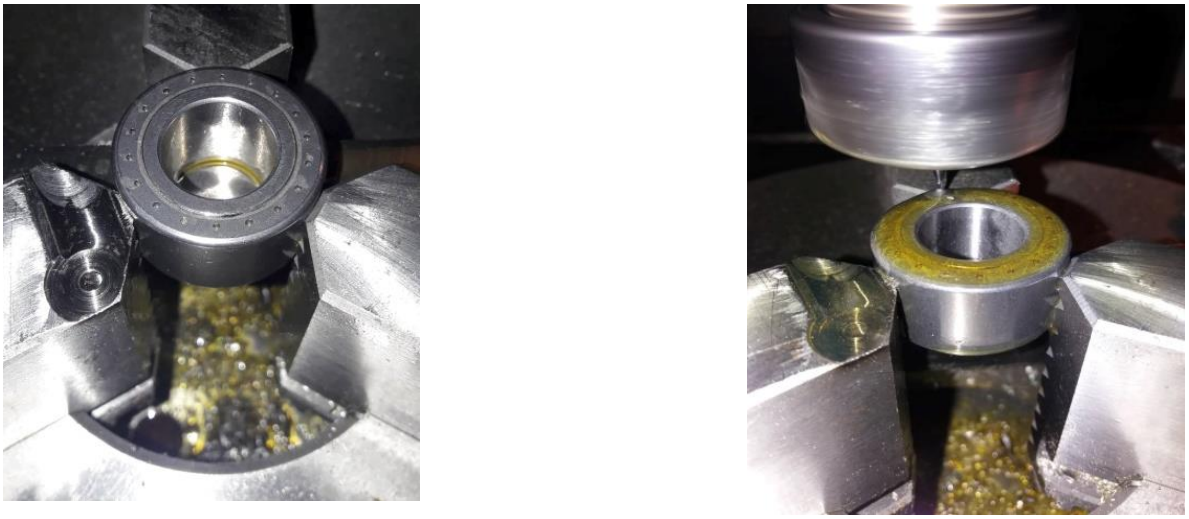

Figure 4.28: Machining of the DAF Roller

To embed the sensor mounted in the M5 grub screw, the roller casing was drilled with a 4.2mm drill and then using an M5 tap, threads were made.

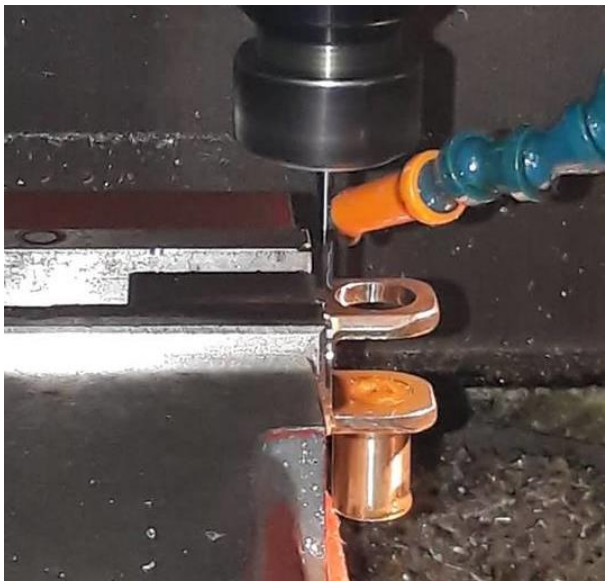

Figure 4.29: Machining of roller casing

Machining the Prius Rollers

For the Prius roller, we had to drill 20 holes, 10 on each side with an offset of 18 degrees, having a depth of 1.05mm. These holes will serve as a housing for the AlNiCo Magnets which will be detected by the GMR sensors.

We needed a reference to keep the exact offset between holes on either side of the roller since the available CNC was unable to drill on both sides without us manually flipping the roller. If this was done, the roller would have been placed at an incorrect position causing an error in the drill positions. Hence, we needed a fixture that would preserve the information of the original coordinates even when flipped and would act a reference to ensure the exact offset between the holes.

Acrylic Center Fitting

We cut an acrylic cylinder of dimensions equal to the inner diameter of the roller and press fitted it inside the roller. After machining one side of the roller, we drilled a 2mm through hole in the acrylic cylinder at 2.5mm from the center. This through hole was aligned with one of the holes in the roller. This would be our reference when the roller was flipped.

Figure 4.30: Acrylic Center Fitting for Realignment

We unfastened the roller and after flipping it we aligned the through hole with the drill. We now fastened the chuck and checked tested for alignment.

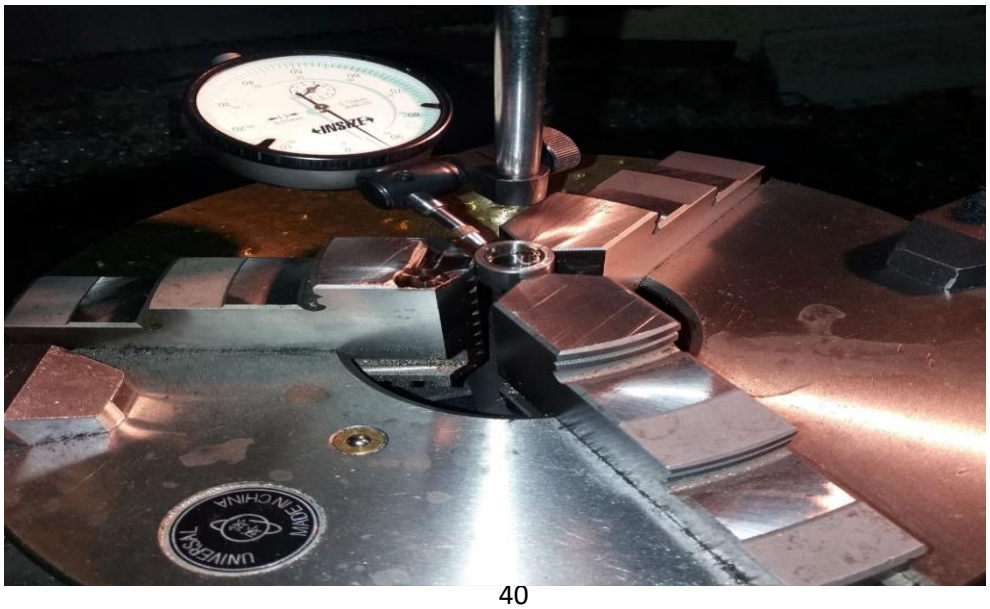

Figure 4.31: Realignment of Roller After Flipping Sides

Now, we had the information of the previous coordinate points. We updated the coordinates with an offset and machined the other side of the roller.

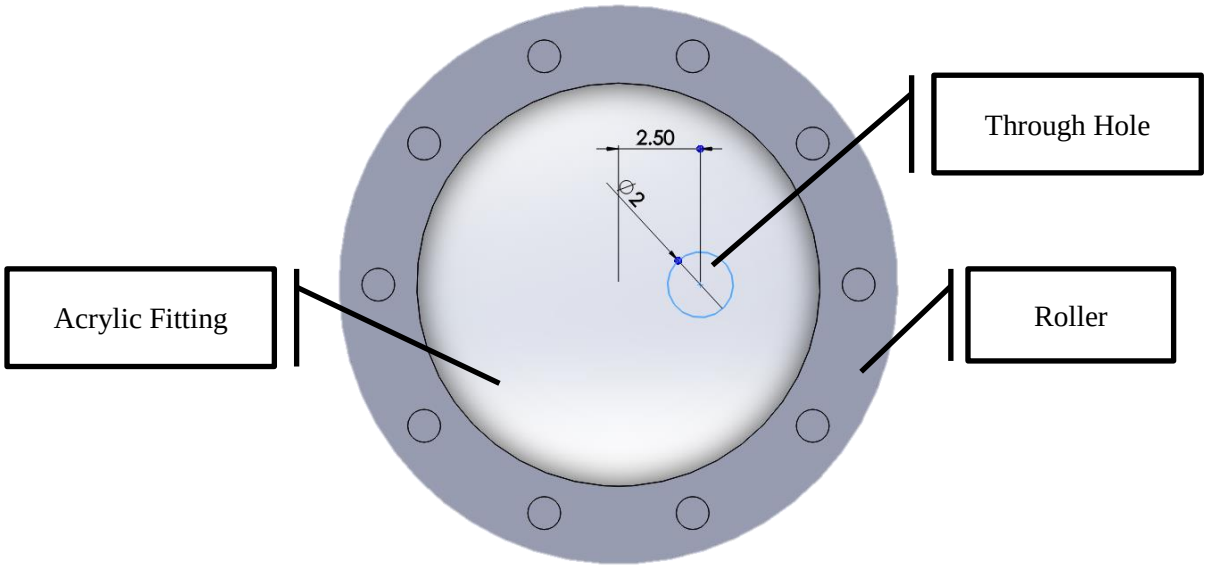

Figure 4.32: Engineering Drawing of Alignment Hole Placement

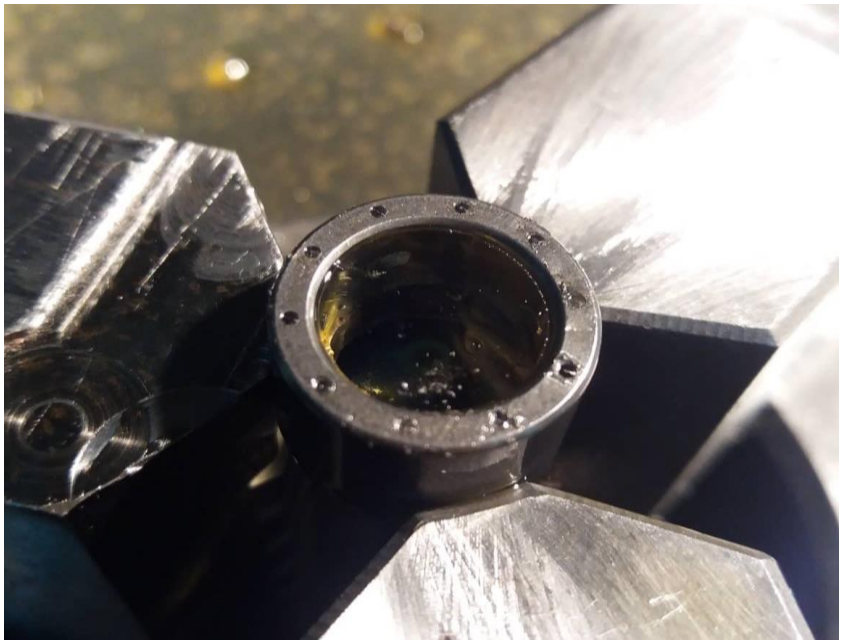

Figure 4.33: Machined Roller

Setup

Our final setups are presented below:

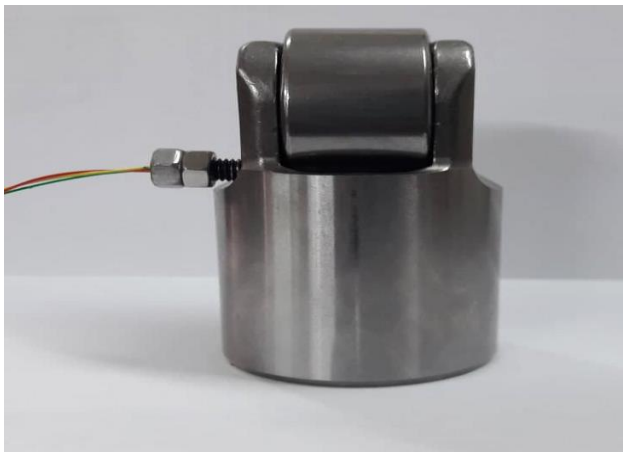

Figure 4.34: Instrumented DAF Truck Tappet Follower

Figure 4.35: Instrumented Toyota Prius Finger Follower

Signal processing: Combining Signals from Two Sensors on Toyota Prius Roller

Two GMR sensors were used to detect magnets on both sides of the Prius roller to improve resolution of signal. As a result of the 10 magnets on each side (with a 90^{o} offset from each other), there were a total of 20 peaks during one complete revolution of the roller. The next step was to combine the signal from the two sensors so that the resultant would give a resolution of 18 degrees for the roller rotation with both signals synchronized.

Ideally when one sensor showed a peak, the other would be zero and this pattern would alternate. However, when the roller was rotated at high speeds, one sensor would show a peak whilst the other one had not gone to zero resulting in signal overlap. As a result, the net signal would show one peak instead of two separate peaks as shown in the image received from the oscilloscope testing.

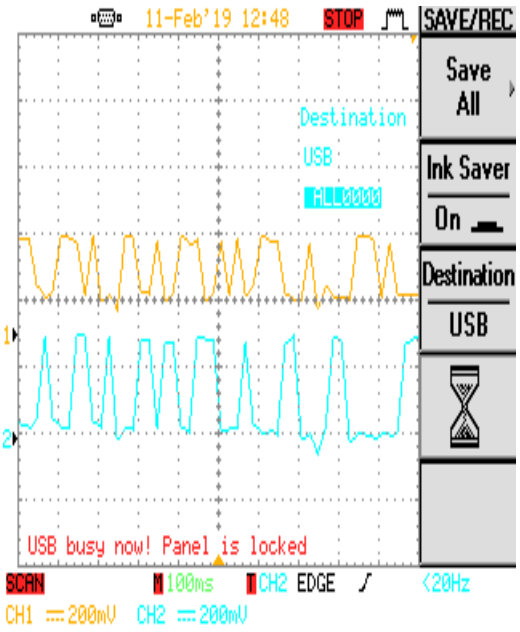

Figure 4.36: GMR Sensor Digital Signal on Oscilloscope

In order to solve this problem, an XOR gate was considered. The input signals of the GMR sensors would be fed at the two inputs of the gate and its output would give the combined output. The idea is that even when two peaks occur simultaneously, the output would go to zero and any error due to the overlap of the previous signal would be removed.

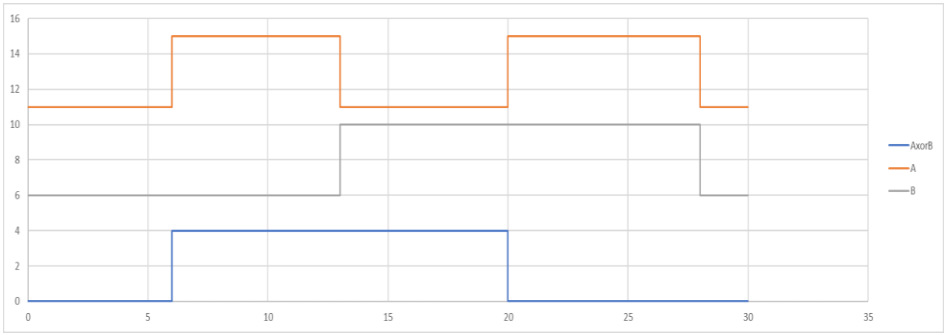

Figure 4.37: XOR Gate Response to Various Inputs

Inputs		Outputs
X	Y	Z
0	0	0
0	1	1
1	0	1
1	1	0

Table 4.3: XOR Truth table

The following circuit schematic was devised which made use of a voltage regulator to ensure a stable voltage was continuously supplied to the GMR sensors along with capacitor to prevent electrical damage. The latter part of the circuit consisted of the above mentioned XOR gate to accumulate the two signals into one.

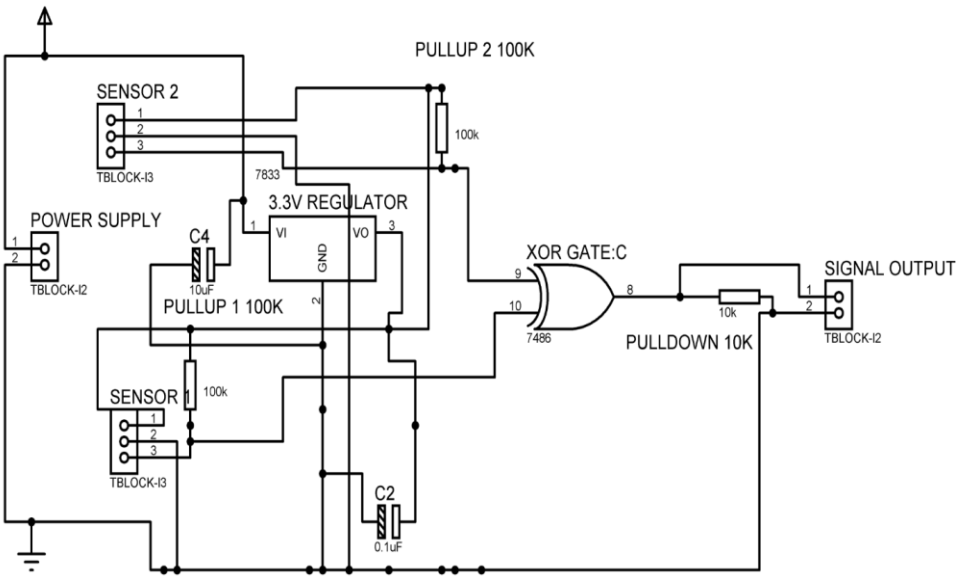

Figure 4.38: PCB Schematic for Signal Accumulation

CHAPTER 5: DATA ACQUSITION

This chapter is divided into two different data acquisition ways to measure instantaneous slip

I. Verify the setup that can detect a sudden change in the speed of rotation of the roller even for a short period of time (instantaneous slip)

II. Place follower inside the engine to measure real time instantaneous roller slip.

Verification Data Acquisition Setup

Frequency Conditioner

We utilized a frequency signal conditioner to convert the digital signal generated by the GMR sensors into an analog signal that manifests the frequency of rotation of the roller.

Since our sensor gives an NPN output, we wired the frequency signal conditioner in the following manner:

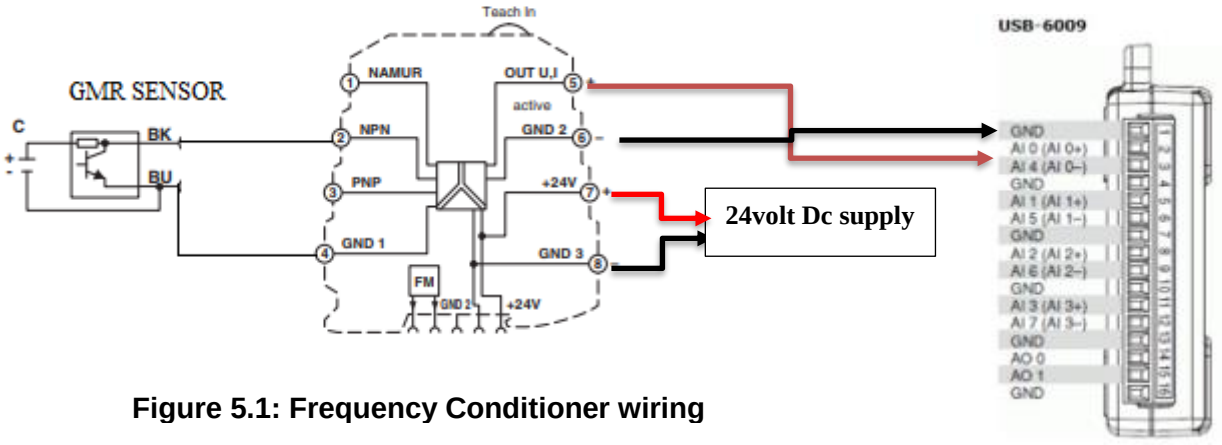

Figure 5.1: Frequency Conditioner wiring

As the roller would rotate, it was important to check how the rotation speed was varying with the cam position and fluctuations in the analogue output from the frequency conditioner would relay that information.

Since the rotating magnets formed a waveform, they could be treated as a square wave. The frequency of rotation of the roller would simply be:

$$Frequency\ of\ DAF\ roller = \frac{Frequency\ of\ DAF\ waveform}{18}$$

$$Frequency\ of\ Prius\ roller = \frac{Frequency\ of\ Prius\ waveform}{20}$$

The frequency conditioner converted the digital signal being input into a frequency being manifesting in the form of an analogue voltage on a scale from 0 to 10V.

The frequency detected on a scale of 0 to 10V was according to the formula:

$$Voltage\ output\ frequency\ conditioner = \frac{Frequency\ In}{Max\ Frequency} \times 10$$

Figure 5.2: Frequency Conditioner Working Principle

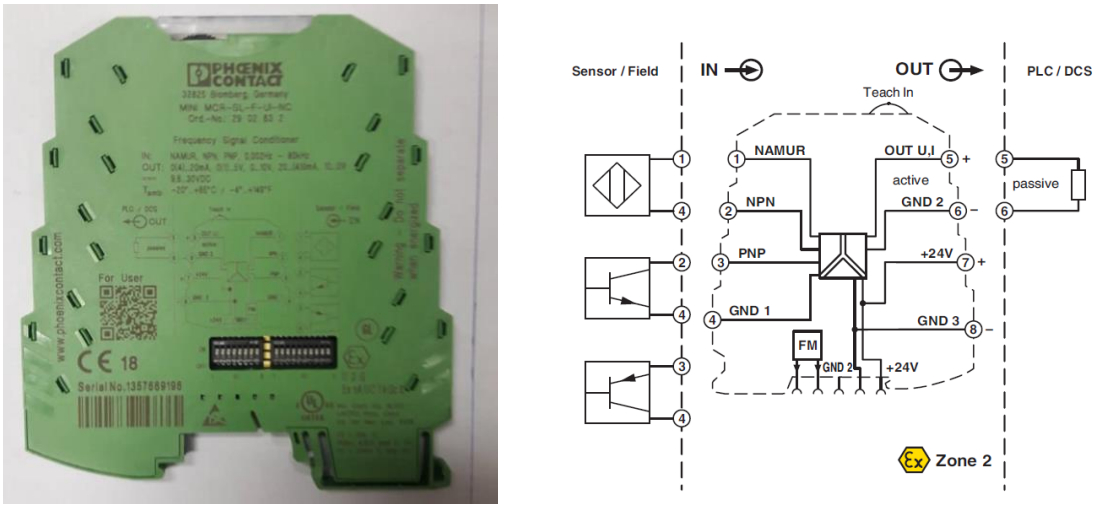

Figure 5.3: Frequency Conditioner Schematic

The wiring was completed, and a test run was conducted. We saw the voltage output from the frequency conditioner increase as the rotation speed of the roller was increased. This was initially done by simply rotating the roller manually. More rigorous testing was then conducted first using a Teflon ring on the roller for verification purposes and then using cam shafts in order to understand the effects of varying surface profiles and surface material on the angular speed of the roller.

Data Acquisition

Once we were able to achieve a digital signal, we had to transfer the signal on a computer system so that we could collect it in the form of data points. For this purpose, we used the NI USB 6009 DAQ card along with the NI LabView software. A counter was implemented which would increase the count by one every time a magnet would be detected.

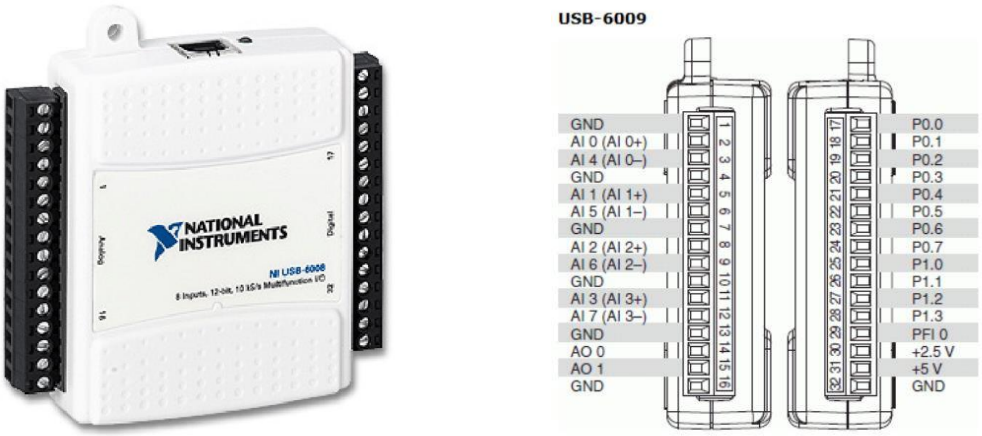

Figure 5.4: DAQ Card NI 6009

In order to ensure that the counter worked without any flaws, we tested the system by rolling the roller a distance equal to its circumference and checking if the counter reached 18 counts (as there were 18 magnets embedded in the case of DAF Tappet Follower)

In order to verify whether a particular frequency of the roller corresponds to the calibrated voltage level, we used a virtual instrument on LabView that detected the frequency and the voltage simultaneously. We measured the frequency of the roller by a DAQ card that takes the voltage signal generated by the GMR sensor as input into one of the analog channels of the DAQ card. We know that as the angular speed of the roller increases, the frequency with which the magnets are detected increases. We employed the Tone Measurement function of the DAQ assistant that utilizes these voltage signals and outputs the frequency. On the other hand, we gave the voltage from the frequency signal conditioner into another analog channel of the DAQ card which is shown directly on a numeric indicator.

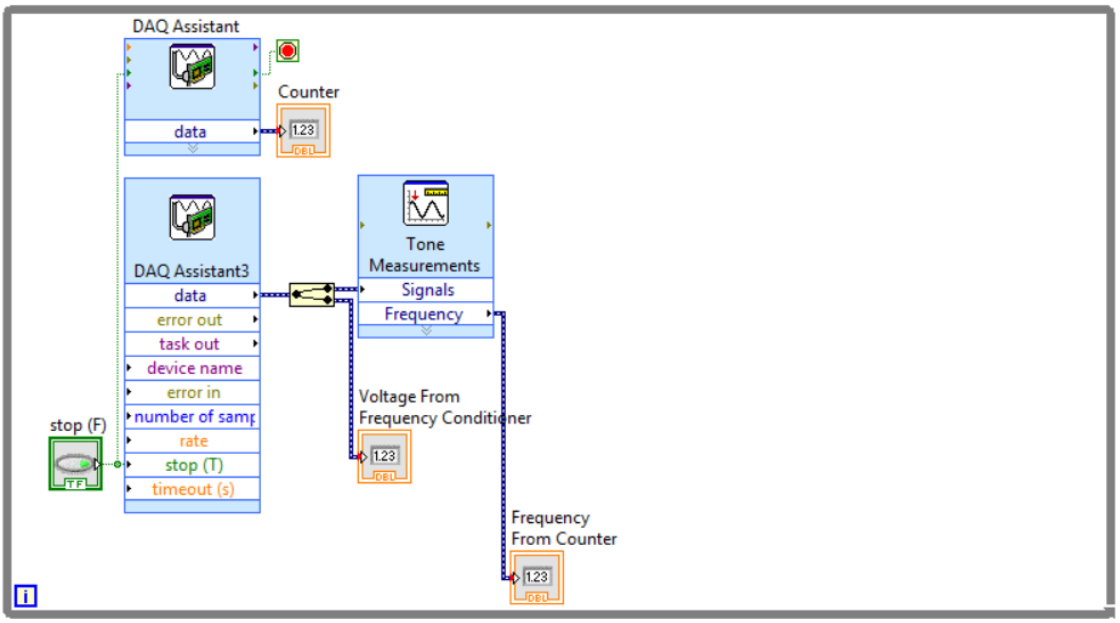

Figure 5.5: LabView Block Diagram

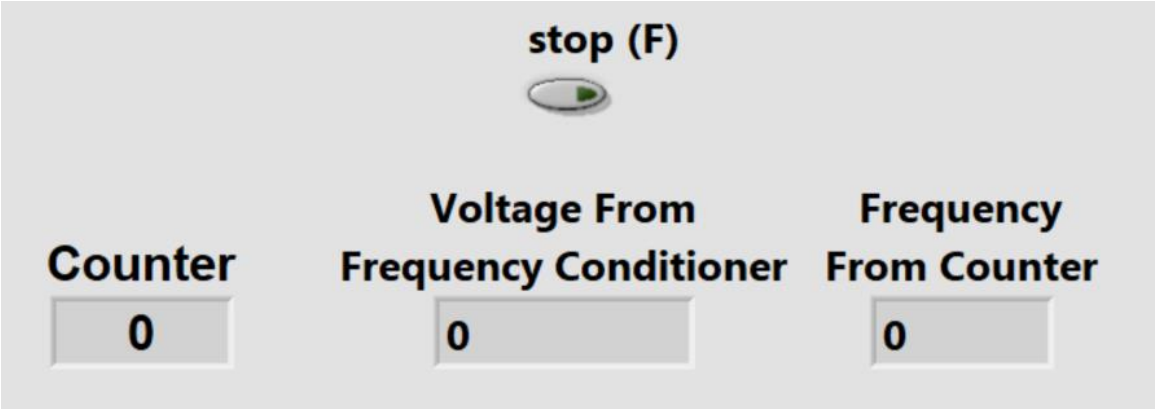

Figure 5.6: LabView Counter

The frequency from the DAQ card had to correspond to the voltage generated by the frequency conditioner in order to ensure correct results were being achieved. This was achieved during our experiments.

The reason a frequency conditioner was used to measure the frequency of the signal from the GMR sensor and not the frequency measurement tool from the DAQ card was because the conditioner had the added capability to eliminate noise giving us a clearer output.

Real time Data Acquisition Setup

All of the data was fed into an NI 9215 DAQ card and NI LabView Software was used to process and store the data. The three parameters that were recorded were the

1. Encoder index pulses (Z channel - 1 peak per cam revolution) to mark start of cam revolution,
2. the encoder incremental pulses (A channel - 720 peaks per cam revolution) to mark degree of cam rotation
3. finally, the accumulated GMR Sensor pulses from XOR Gate (20 peaks per roller revolution).

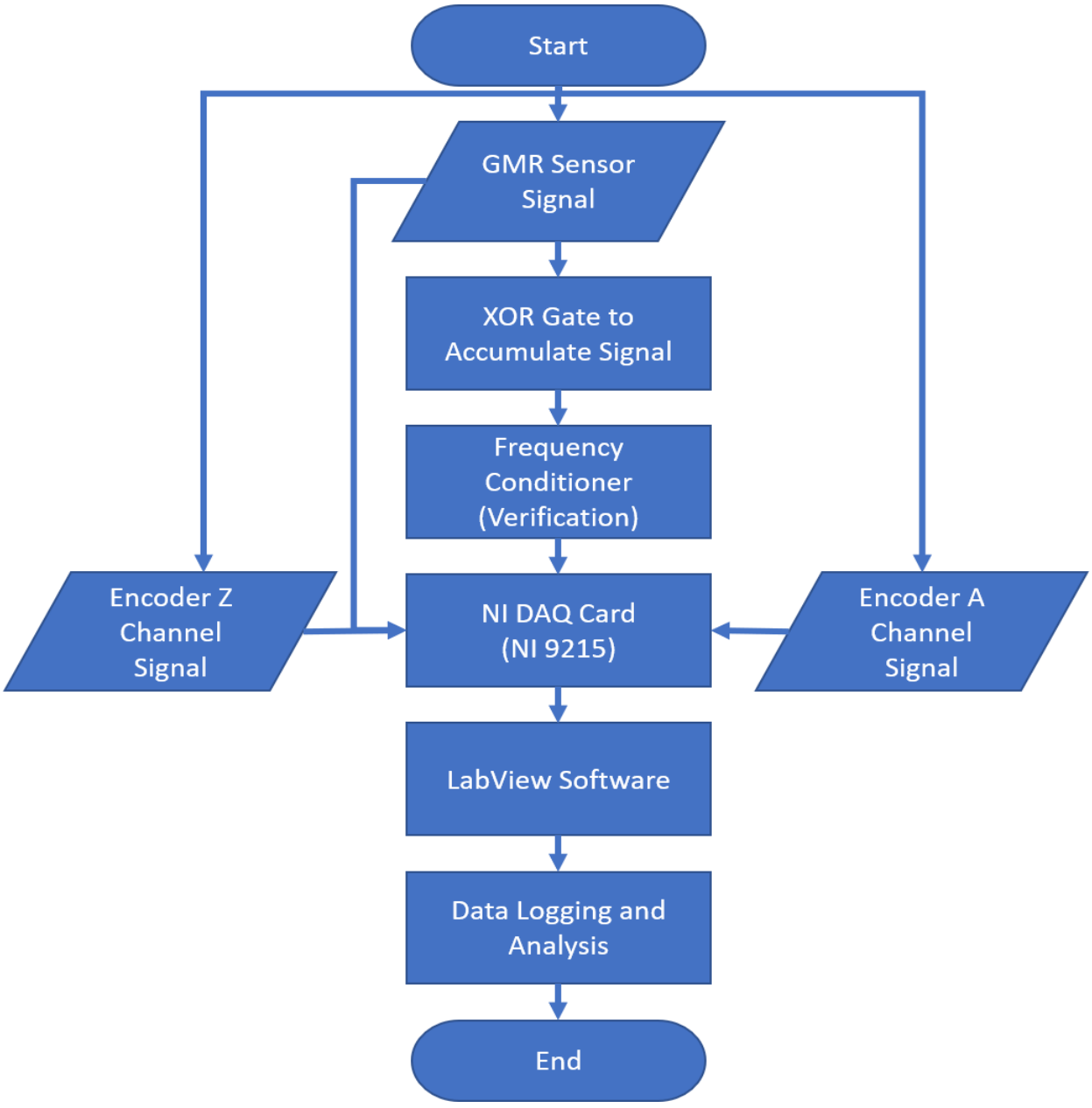

Figure 5.7: Data Acquisition Process Flow chart

It to be noted that the index pulse from the Z channel of the encoder could give a signal at any cam orientation, however we wanted the index pulse to mark the start of a revolution when the cam had fully depressed the valve into its open position. For this we manually aligned the cam shaft in such a way that it would correspond to the index pulse at the valve open position. Further details can be found in Chapter 6 and Dr Khurram thesis.

All the collected data was logged into a TDMS file and post processing was done using spreadsheets.

LabVIEW Code for Real time Instantaneous Roller slip

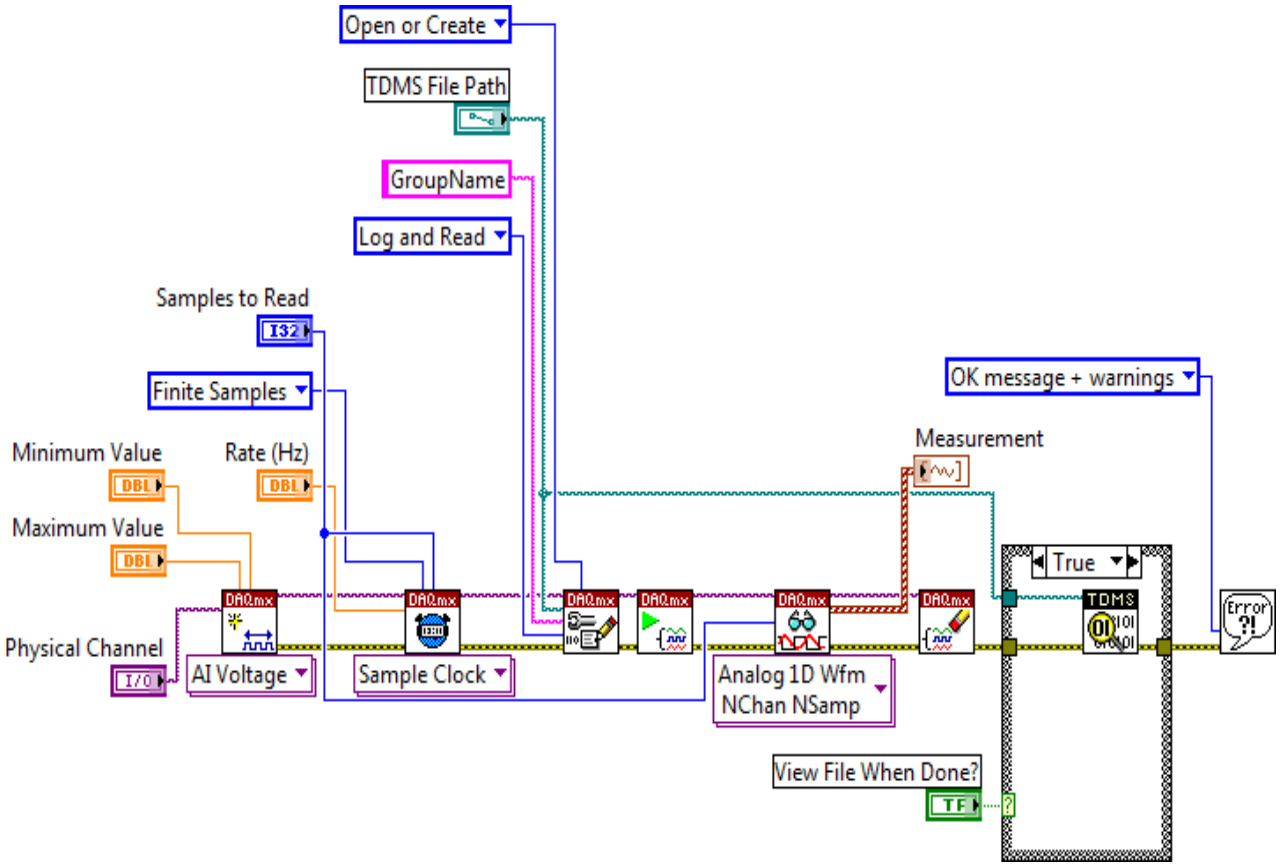

Figure 5.8: Block Diagram for Real time Instantaneous Roller slip

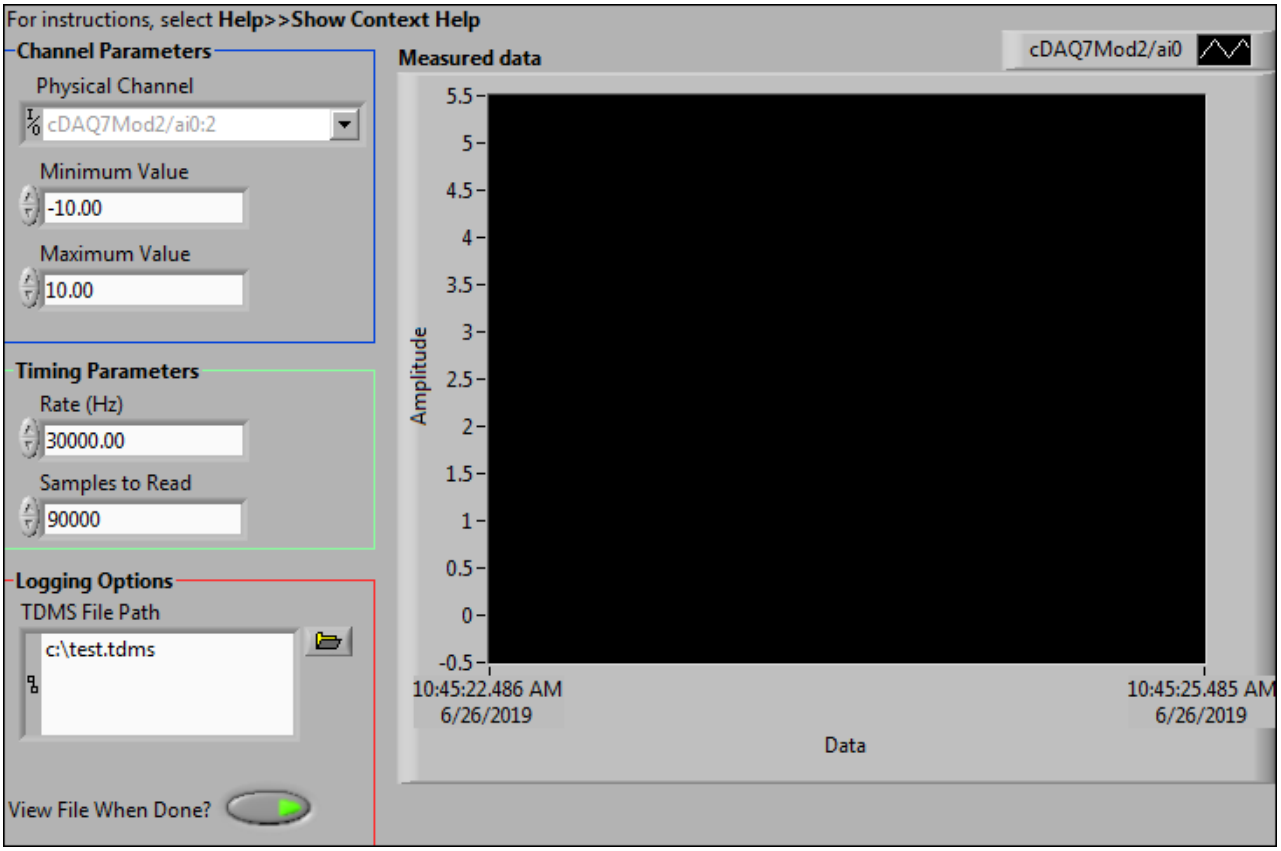

Figure 5.9: Block Diagram for Real time Instantaneous Roller slip

Wiring Diagram for Real time Instantaneous Roller slip

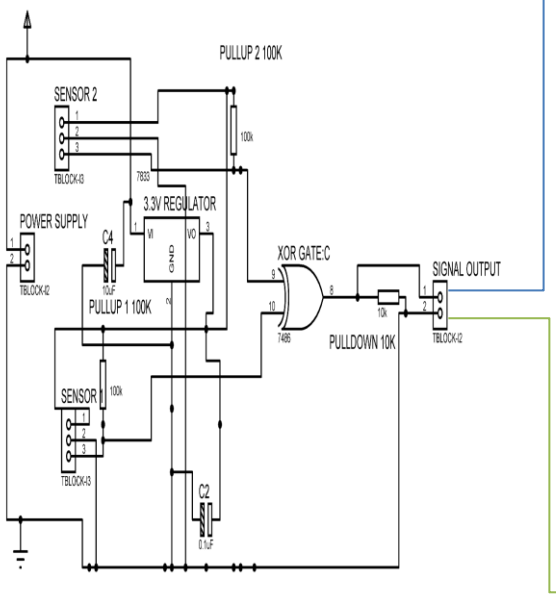

Figure 5.10: Roller GMR sensor output from PCB

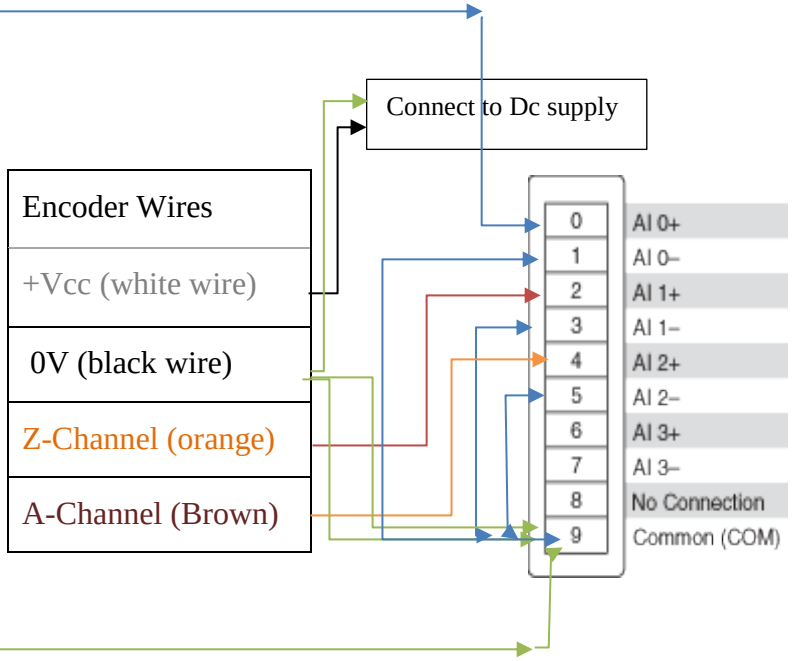

Figure 5.11: Encoder and NI 9215 Pinouts

CHAPTER 6: VERIFICATION AND RESULTS

Validation of Slip Data

Before we started the complete testing for instantaneous slip of the roller, we needed to verify if the frequency conditioner could detect a sudden change in speed of rotation of the roller even for a short period of time. For the roller was to be rolled on by a Teflon ring attached to the shaft of the motor. The roller was supported by a vice to ensure it was in firm contact with the Teflon ring. The setup is shown.

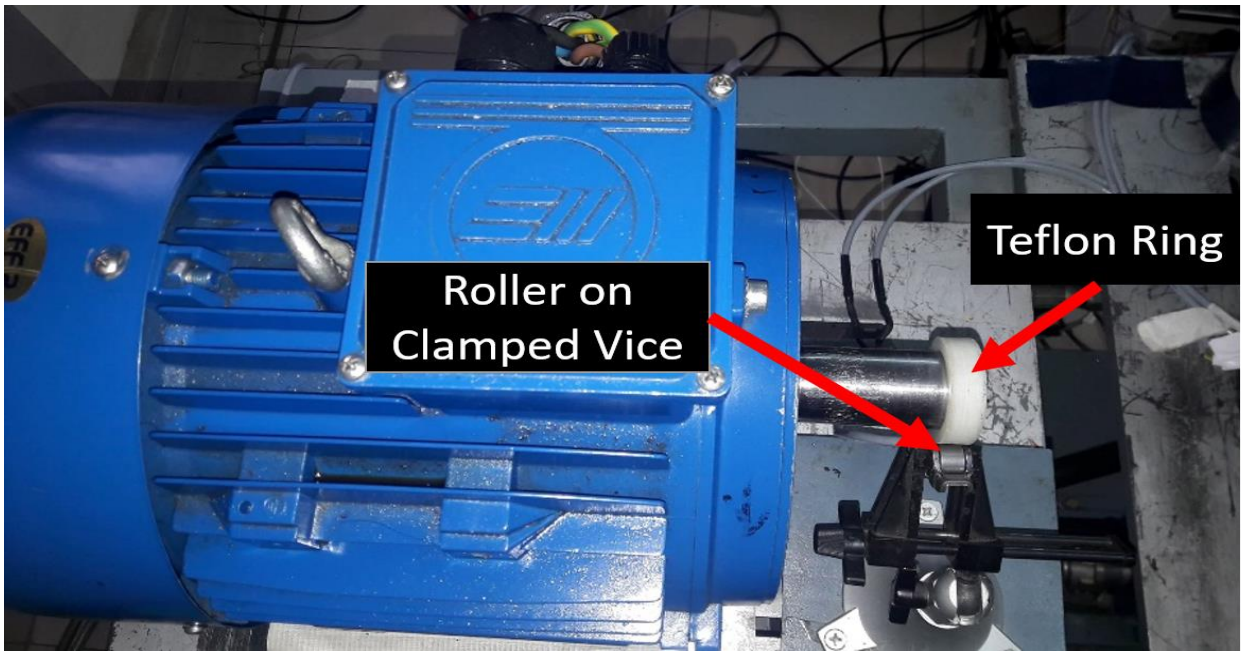

Figure 26.1: Slip Validation Setup

The diameter of the Teflon ring was 52mm which meant a ratio of 3.06 between the Teflon ring and the roller. Assuming that no slip occurred, the frequency of the roller would then be

$$Frequency\ of\ Roller\ (Hz) = \frac{Speed\ of\ Motor(rpm)}{60} \times 3.06$$

Since there were 20 magnets in the roller, the frequency detected by the frequency conditioner would then be 20 times the frequency of the roller in Hz.

We ran our validation tests at a motor speed of 200 RPM. At 200 RPM the frequency detected by the frequency conditioner would be

$$Frequency\ detected\ by\ frequency\ conditioner = \frac{Motor\ RPM}{60} \times Dia\ Ratio \times No.\ of\ Magnets$$

$$Frequency\ detected\ by\ frequency\ conditioner = \frac{200}{60} \times 3.06 \times 20 = 200\ Hz$$

$$Voltage\ output\ by\ frequency\ conditioner$$
$$= Frequency\ detected\ by\ frequency\ conditioner\ \times \frac{10}{Max\ set\ frequency}$$

Accordingly, we set the maximum frequency of the frequency conditioner to 400 Hz which meant a voltage of 5V should be received as output.

$$Voltage\ output\ by\ frequency\ conditioner = 200\ \times \frac{10}{400} = 5V$$

The following graph was generated

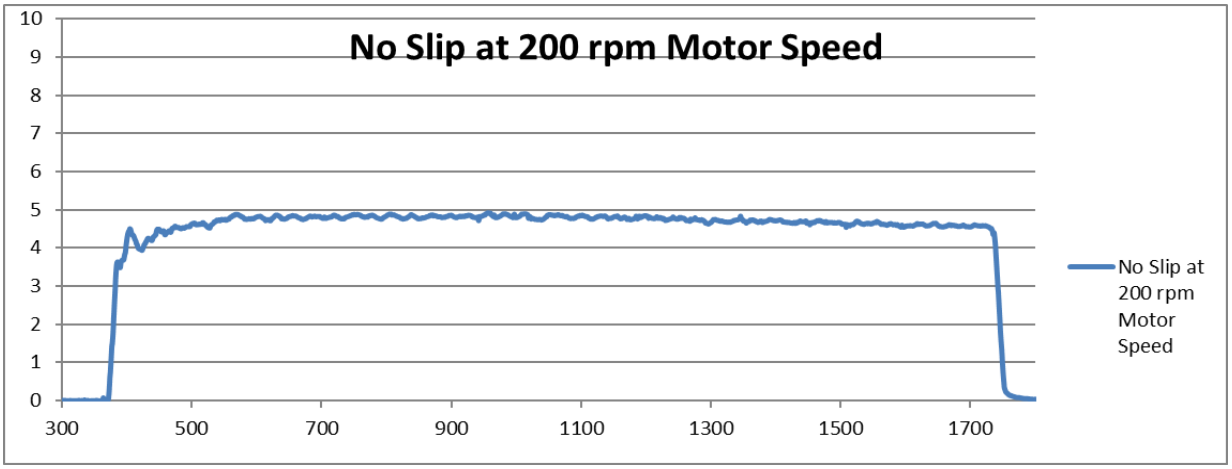

Figure 6.2: Frequency Conditioner Output No Slip 200 RPM Motor Speed

Next, we induced slips manually by tapping the roller with a thin screw driver. The voltage from the frequency conditioner had to drop in order to show that the roller had slowed down for an instant and hence register the slip. This is shown in the picture below.

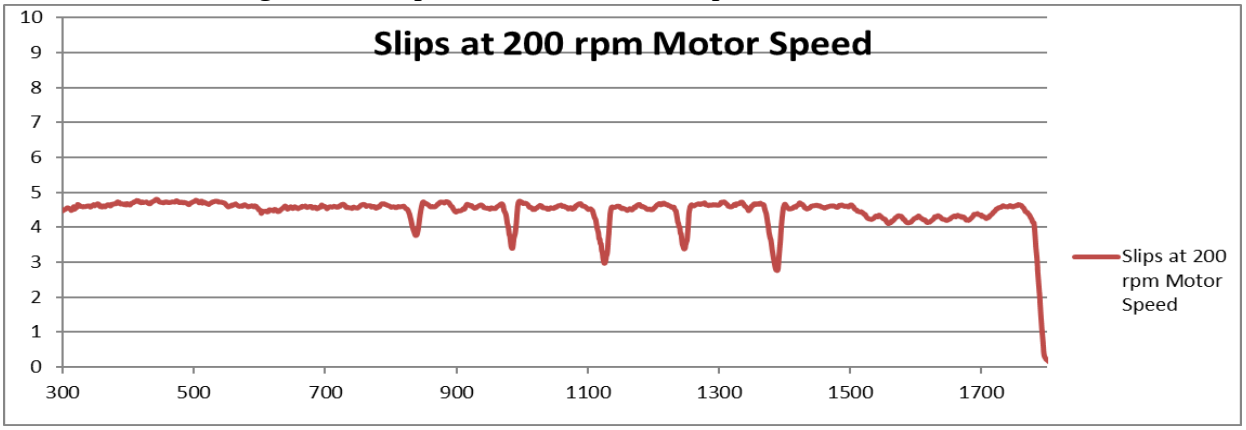

Figure 6.3: Frequency Conditioner Output with Slips 200 RPM Motor Speed

The graph shows 5 drops in voltage which correspond to the five taps made on the roller. This verifies that the frequency conditioner was registering instantaneous slips in the roller's interaction with the Teflon ring.

Finding Valve Open Position Relative to Index Pulse

In order to better analyze the data collected from the experiments i.e. running the instrumented roller in the engine at different speeds, it was necessary to locate top position of the cam lobe as it pressed the valve spring to its lowest point with respect to index mark of the motor. This way, we can study the slippage phenomenon at top position of the cam by superimposing its extreme position as another index mark on the experimentally collected data as shown in the graph below:

Setup

The dial indicator was installed in such a manner that the contact point on the spindle of dial indicator was seated firmly against the valve spring retainer which allowed easy monitoring of the vertical movement of the valve against the spring tension. To find lift of the cam, we required a dial gauge with an electromagnetic base. We tried to find several positions in the engine head to place the dial gauge but due to strict geometric constraints we could not find any position in which the gauge head would touching the valve spring of the instrumented roller without moving from its position. Hence, we fixed a clamp-on vice on outer body of the rig and held a steel plate *(reference to mild steel plate topic)* with it. We placed the dial gauge on the steel plate and positioned it so that the gauge head was pressed against the valve spring when the cam is at its extreme position i.e. the bottom dead center. In this way, we located top position of the cam with help of the dial gauge.

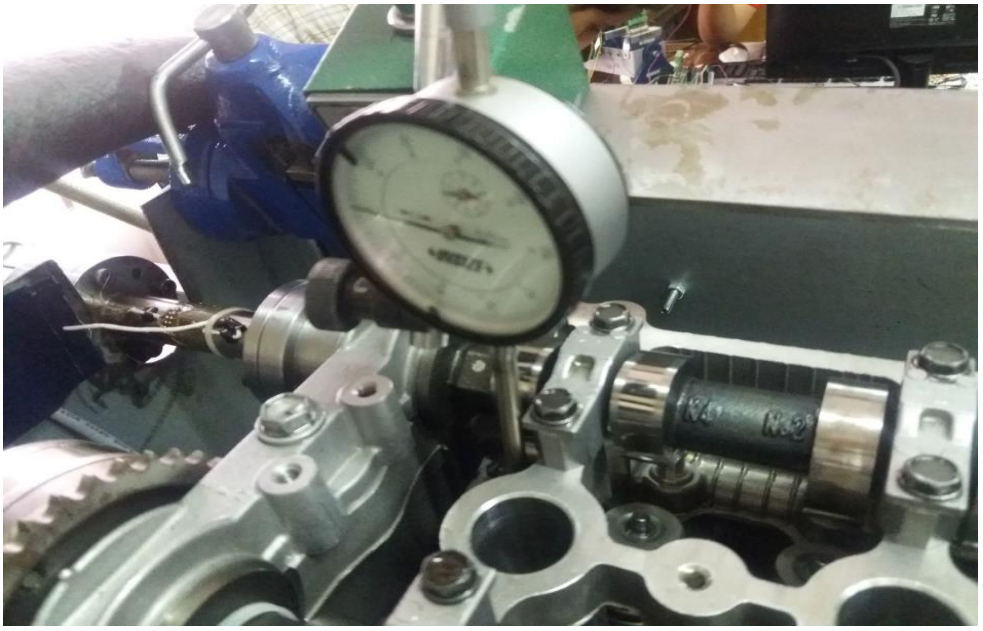

Figure 6.4: Index Relative to Top Dead Center Measurement

In the next step, we found how far Z index of the motor is situated with respect to the bottom dead center. We connected 'A' channel of the encoder, which gives 720 pulses per revolution, with a DAQ counter. We also connected Z channel of the encoder in an analog input of the DAQ card. In a LabView VI, we simultaneously checked the count and the pulse from Z channel as we manually rotated the camshaft. As soon as we got a digital high from the Z channel, we noted value from the counter. This value is related to angle of the camshaft as:

$$Angle\ between\ Z\ index\ and\ extreme\ position\ of\ the\ cam\ in\ degrees = \frac{Value\ from\ the\ counter}{2}$$

We started by making sure the valve was in open position as at that position the dial gage would give us the minimum value as it would be minimally pressed and. We then performed rotated the camshaft both clockwise and counter-clockwise until the index pulse was achieved multiple times to get an average value. The sum of clockwise and counter clockwise rotations should ideally be 720 according to the encoder's resolution. The results from the experiment are tabulated below:

No. of Pulses in Counter Clockwise Rotation	Counter Clockwise Degree offset	No. of Pulses in Clockwise Rotation	Clockwise Degree offset
508	254.0	221	110.5
505	252.5	222	111.0
497	248.5	219	109.5
503	251.5	223	111.5

Table 3: Measurements for Offset Between Top Dead Center and Index Pulse

We can see that the angles from both experiments add up to approximately 360^{o}. This verifies the results of the experiment. Slight error can be explained as a human error because of the manual nature of the experiment. However, this error is negligible in our case. Finally, we mapped values of the angle during post processing in excel sheet.

Another way of doing this is the top of cam lift was estimated with the help of dial indicator, once the nose of cam was fully in the downward direction thereby compressing the spring completely to open the valve fully. At the same very position, the index pulse of the optical encoder was synchronized to appear at the cam nose position. It can be realized that the vertical position of the valve changes very slowly at the camshaft nose area hence the exact marking of top of cam lift position is relatively difficult. The reading at the dial gauge gave estimated accuracy of + 0.4 degree of camshaft angle at the required position. At the same very point, the camshaft and the encoder shaft were locked together.

In this case our index pulse is synchronized with cam nose which means valve is fully lifted/open at 0 degree (index pulse starts). But in actual our engine cam nose is fully open at 180 degree which can be seen in figure 6.5 below. So, in post processing we would shift raw data from 0 degree to 180 degree.

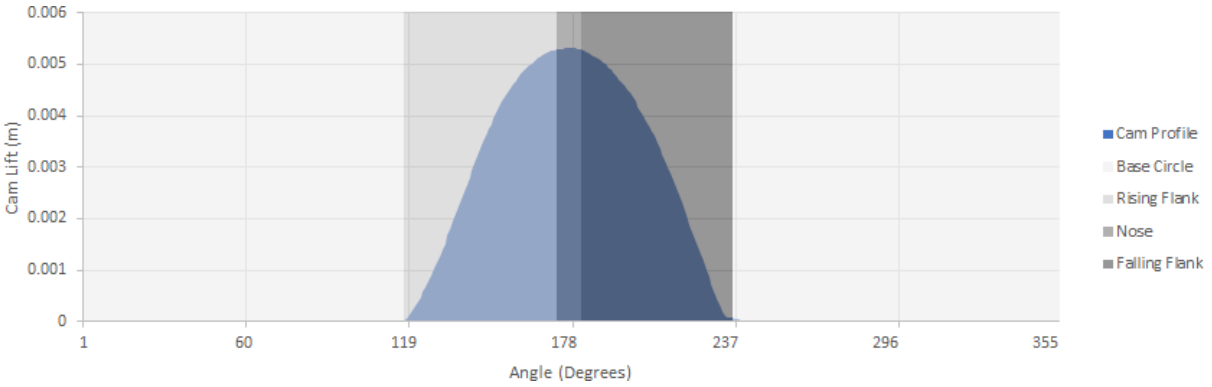

Figure 6.5: Toyota Prius Engine Cam lift profile

It should be noted that this experiment is valid only for a specific alignment of the camshaft. If the camshaft is opened, this experiment must be performed again as the position of the index with respect to the valve open position will have changed.

Real time Experimentation Results.

Once it was verified that our instrumentation method was correctly detecting instantaneous slips, the setup was put into the Toyota Prius 1NZK Engine head. The setup is shown in Figure 6.6.

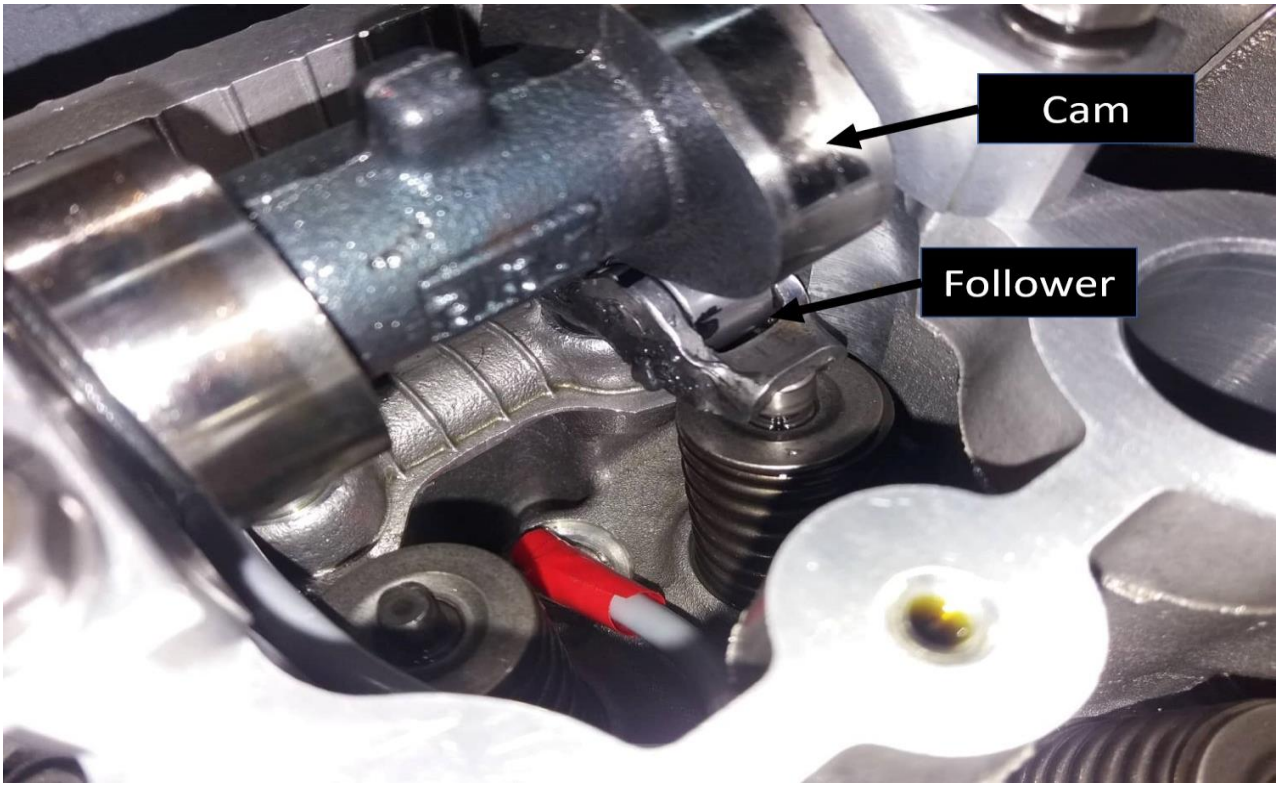

Figure 6.6: Cam and Follower in Engine Head

No Slip Condition Testing

Before we started measuring slip in the engine, it was important to check the data under ideal circumstances. For this purpose, oil was completely removed from the engine head and the cam was rotated at a very slow speed of 45 RPM. The raw data for all three peaks is shown in Figure 17 a. We can see that there are exactly 45 GMR sensor peaks between two consecutive index pulse peaks showing that no slip occurred. In order to check how the speed varies, we measure the number of encoder A channel peaks between two consecutive GMR sensor peaks. Ideally, over the course of one revolution, if the cam radius were constant, each consecutive GMR sensor peak should have 720/45 = 16 peaks. We plot the graph for the number of A channel peaks between consecutive GMR sensor peaks against the angle of cam to get the results shown in Figure 17 b. We see that from 0 to 120 degrees the number of peaks is constant at roughly 16 as stated earlier however we see a dip from 120 to 250. This corresponds to the Rising Flank, Nose

and Falling Flank of the cam. As mentioned previously, because these three regions have a different profile, the radius in contact with the roller changes. The graph shows a reduction in encoder peaks meaning the roller is rotating at a faster pace than it did at the base circle of the cam. This is manifested in the form of lesser number of encoder A channel peaks being registered between consecutive GMR sensor peaks in between 120 degrees to 240 degrees.

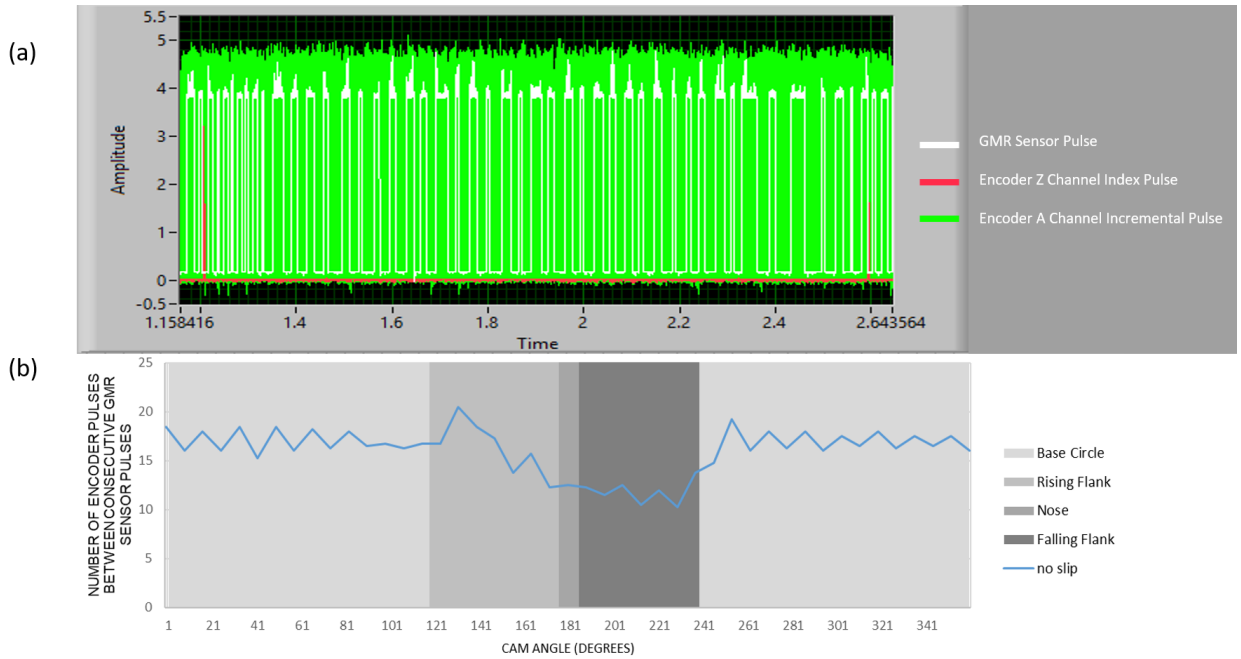

Figure 6.27: (a) No Slip Condition Raw data (b) Number of Enc A pulse between Consecutive GMR sensor Pulse

Slip Condition Testing

For slip condition testing, oil was pumped at 2 bars into the engine head and the cam was rotated at different speeds.

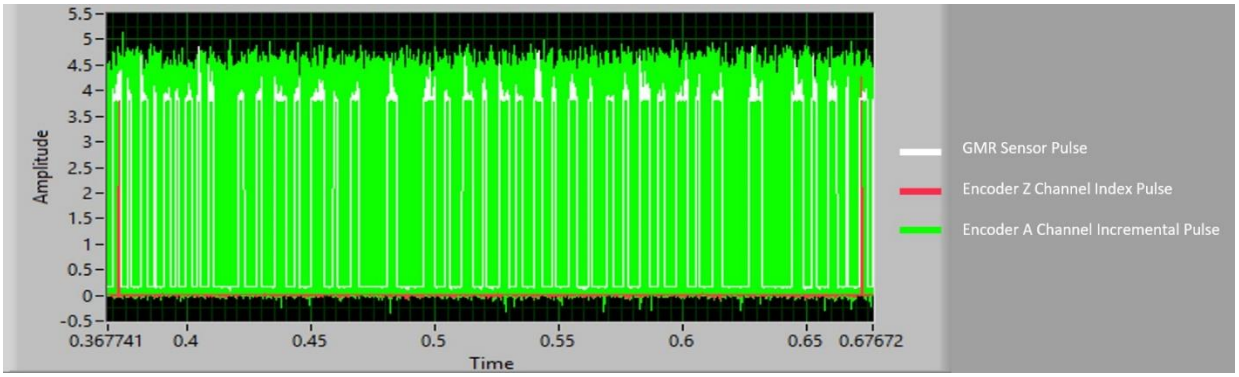

Figure 6.7: shows the raw peaks for 200 rpm cam speed.

The same data was plotted as number of A channel peaks between consecutive GMR sensor peaks and the result was super imposed on the no slip graph as shown in Figures

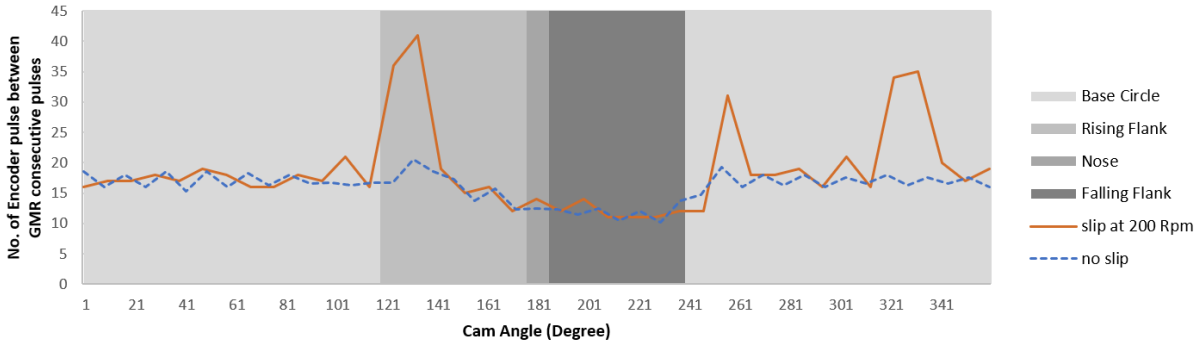

Figure 6.8: Instantaneous Slip at 200Rpm

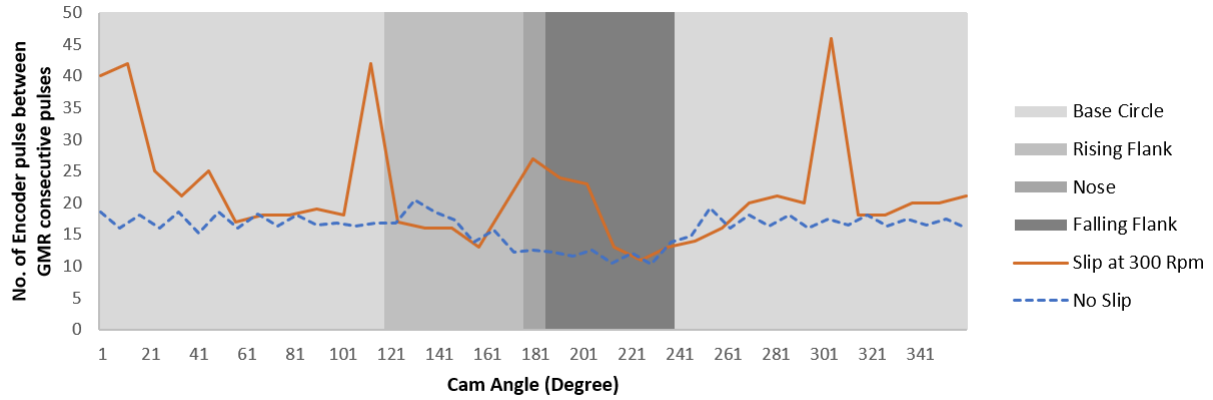

Figure 6.9: Instantaneous Slip at 300Rpm

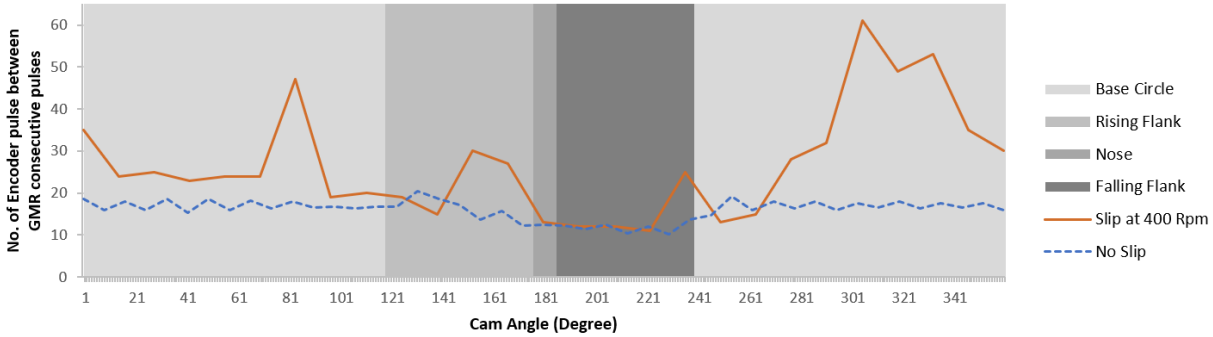

Figure 6.10: Instantaneous Slip at 400Rpm

From the above data, we can see that even under slip conditions, the roller speed increases when the cam radius deviates from the base circle. The two graphs are almost ideal; however, a significant variation can be seen in the three peaks on the slip graph. The peaks effectively mean that at certain positions the roller halted however the cam moved ahead thus the encoder A channel pulses kept registering but the next GMR sensor peak came late.

Another way to observe that slip occurred was to count the number of GMR sensor pulses between two index pulses from the Z channel of the encoder. We saw 45 pulses in the no slip condition however the pulses reduced to 38 at 200 rpm to 33 at 300 rpm and finally to 25 at 400 rpm. This meant that as the cam speed increased, there was an increase in instantaneous slip between the roller and the cam. This is easily observable in the amplitude of the slip peaks in the graphs shown before. The amplitude of number of A channel encoder peaks was 40 at 200 rpm however this increased to 45 at 300 rpm and 60 at 400 rpm showing greater slippage.

We can also see negative slip, that is the roller moving at higher speeds right after 120 and 240 degrees. This is because the roller encounters a sudden change in speed as the rising flank starts (at 120 degrees) and the falling flank ends (at 240 degrees) and thus experiences sudden acceleration. Its own inertia however keeps it from suddenly changing speeds due to which we see the roller slide ahead of the cam at these instances.

Our Thesis focuses on the technique to instrument an end pivoted roller to measure instantaneous slip, further work can be done by performance-based evaluation of the system using the same instrumentation technique under different lubrication oils, temperatures, surface coatings and cam profiles.

CHAPTER 7: CONCLUSION

With the help of this method of instrumenting rollers in engines, we can now investigate numerous tribological effects. This also required minimal changes to the actual assembly and hence the errors that appear due to the process of instrumentation are at a minimum. The method leads to adding new data into research which can help engineers design better cam and roller profiles and choose superior materials. The same instrumentation method can also be applied to different types of roller followers other than the end-pivoted configuration. Further work can be conducted by collecting similar data across various other variables such as different engine conditions, different lubricating agents and different surface coatings. This would allow us to steadily reach optimal engine performance conditions.

REFERENCES

[1] European Union. Reducing CO2 emissions from heavy-duty vehicles, https://ec.europa.eu/clima/policies/transport/vehicles/heavy, Retrieved: 25-05-2018.

[2] European Union. Paris agreement, https://ec.europa.eu/clima/policies/international /negotiations/paris, Retrieved: 25-05-2018.

[3] B. Andersson. Paper xviii (iii) Company perspectives in vehicle tribology-Volvo. *Tribology Series*, 18:503–506, 1991.

[4] U. Abdullah, M. Bhutta, M. Huzaifa Najeeb, M. Khurram, R. Ahmad Mufti, and S. Shah, *Experimental Evaluation of Mean Friction in End Pivoted Roller Follower Valvetrain*, 2017.

[5] M. Khurram, R. Mufti, R. Zahid, N. Afzal, and M. Bhutta, *Experimental measurement of roller slip in end-pivoted roller follower valve train* vol. 229, 2015.

[6] D. Dowson, P. Harrison, C. Taylor, and G. Zhu. Experimental observation of lubricant film state between a cam and bucket follower using the electrical resistivity technique. In *Proceedings of the Japan International Tribology Conference*, pages 119–124, 1900.

[7] G. Zhu. *A theoretical and experimental study of the tribology of a cam and follower*. PhD thesis, The University of Leeds, Leeds, The United Kingdom, 1988.

[8] P. Duffy. An experimental investigation of sliding at cam to roller tappet contacts. Technical report, SAE Technical Paper 930691, 1993.

[9] J. Lee and D. Patterson. Analysis of cam/roller follower friction and slippage in valve train systems. Technical report, SAE Technical Paper 951039, 1995.

[10] B. Gecim. Lubrication and fatigue analysis of a cam and roller follower. *Tribology Series*, 14:91–100, 1989.

[11] J. Matthews and F. Sadeghi. Kinematics and lubrication of camshaft roller follower mechanisms. *Tribology Transactions*, 39(2):425–433, 1996.

[12] Y. Chiu. Lubrication and slippage in roller finger follower systems in engine valve trains. *Tribology transactions*, 35(2):261–268, 1992.

[13] F. Ji and C. Taylor. A tribological study of roller follower valve trains. part 1: A theoretical study with a numerical lubrication model considering possible sliding. *Tribology Series*, 34:489–499, 1998.

[14] S. Bair and W. Winer. Paper vi (v) a technique for measuring roller follower skidding on automotive camshafts. *Tribology Series*, 18:157–162, 1991.

[15] A. Turturro, R. Rahmani, H. Rahnejat, C. Delprete, and L. Magro. Assessment of friction for cam-roller follower valve train system subjected to mixed non-newtonian regime of lubrication. In *ASME 2012 Internal Combustion Engine Division Spring Technical Conference*, pages 917–923. American Society of Mechanical Engineers, 2012.

[16] M. Khurram, R. Mufti, R. Zahid, N. Afzal, M. Bhutta, and M. Khan. Effect of lubricant chemistry on the performance of end pivoted roller follower valve train. *Tribology International*, 93:717–722, 2016.

[17] M. Umar, R. Mufti, and M. Khurram. Effect of flash temperature on engine valve train friction. *Tribology International*, 118:170–179, 2017.

[18] M. Abdullah, S. Shah, M. Bhutta, R. Mufti, M. Khurram, M. Najeeb, W. Arshad, and K. Ogawa. Benefits of wonder process craft on engine valve train performance. *Proceedings of the Institution of Mechanical Engineers, Part D: Journal of Automobile Engineering*, Epub March 12, 2018. DOI:10.1177/0954407018760935.

[19] P. Lindholm, C. Spiegelberg, S. Andersson, and S. Bjorklund. Contact conditions in a cam and roller contact. In *World Tribology Congress WTC2001*, page 4, 2001.

[20] R. Mufti and A. Jefferies, *Novel method of measuring tappet rotation and the effect of lubricant rheology* vol. 41, 2008.

[21] K. Kapser, M. Weinberger, W. Granig, and P. Slama, "GMR Sensors in Automotive Applications," ed, 2013, pp. 133-156.

[22] C. P. O. Treutler, *Magnetic Sensors for Automotive Applications* vol. 91, 2001.